

Synthesis and structure-activity relationship of nitrile-based cruzain inhibitors incorporating a trifluoroethylamine-based P2 amide replacement

Juliana C. Gomes, Lorenzo Cianni, Jean Ribeiro, Fernanda dos Reis Rocho, Samelyn da Costa Martins Silva, Pedro Henrique Jatai Batista, Carolina Borsoi Moraes, Caio Haddad Franco, Lucio H.G. Freitas-Junior, Peter W. Kenny, Andrei Leitão, Antonio C.B. Burtoloso, Daniela de Vita, Carlos A. Montanari

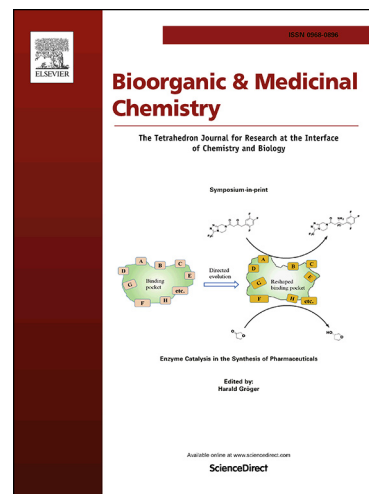
PII: S0968-0896(19)31004-1
DOI: <https://doi.org/10.1016/j.bmc.2019.115083>
Reference: BMC 115083

To appear in: *Bioorganic & Medicinal Chemistry*

Received Date: 23 June 2019
Revised Date: 22 August 2019
Accepted Date: 26 August 2019

Please cite this article as: Gomes, J.C., Cianni, L., Ribeiro, J., dos Reis Rocho, F., da Costa Martins Silva, S., Batista, P.H.J., Moraes, C.B., Franco, C.H., Freitas-Junior, L.H.G., Kenny, P.W., Leitão, A., Burtoloso, A.C.B., de Vita, D., Montanari, C.A., Synthesis and structure-activity relationship of nitrile-based cruzain inhibitors incorporating a trifluoroethylamine-based P2 amide replacement, *Bioorganic & Medicinal Chemistry* (2019), doi: <https://doi.org/10.1016/j.bmc.2019.115083>

This is a PDF file of an article that has undergone enhancements after acceptance, such as the addition of a cover page and metadata, and formatting for readability, but it is not yet the definitive version of record. This version will undergo additional copyediting, typesetting and review before it is published in its final form, but we are providing this version to give early visibility of the article. Please note that, during the production process, errors may be discovered which could affect the content, and all legal disclaimers that apply to the journal pertain.



Synthesis and structure-activity relationship of nitrile-based cruzain inhibitors incorporating a trifluoroethylamine-based P2 amide replacement

Juliana C. Gomes^a, Lorenzo Cianni^b, Jean Ribeiro^b, Fernanda dos Reis Rocho^b, Samelyn da Costa Martins Silva^b, Pedro Henrique Jatai Batista^b, Carolina Borsoi Moraes^c, Caio Haddad Franco^c, Lucio H. G. Freitas-Junior^c, Peter W. Kenny^b, Andrei Leitão^b, Antonio C. B. Burtoloso^a, Daniela de Vita^{*b}, Carlos A. Montanari^{*b}

^aInstituto de Química de São Carlos, Universidade de São Paulo, São Carlos, São Paulo, Brazil

^bGrupo de Química Medicinal do IQSC/USP, Instituto de Química de São Carlos, Universidade de São Paulo, São Carlos, São Paulo, Brazil

^cDepartamento de Microbiologia, Instituto de Ciências Biomédicas, Universidade de São Paulo, São Paulo, Brazil

Contact details: Carlos.Montanari@usp.br, Department of Chemistry and Molecular Physics

Institute of Chemistry of São Carlos University of São Paulo, Av. Trabalhador Sancarlene, 400, 13566-590 - São Carlos / SP

Abstract

The structure-activity relationship for nitrile-based cruzain inhibitors incorporating a P2 amide replacement based on trifluoroethylamine was explored by deconstruction of a published series of inhibitors. It was demonstrated that the P3 biphenyl substituent present in the published inhibitor structures could be truncated to phenyl with only a small loss of affinity. The effects of inverting the configuration of the P2 amide replacement and linking a benzyl substituent at P1 were observed to be strongly non-additive. We show that plotting affinity against molecular

size provides a means to visualize both the molecular size efficiency of structural transformations and the non-additivity in the structure-activity relationship. We also show how the relationship between affinity and lipophilicity, measured by high-performance liquid chromatography with an immobilized artificial membrane stationary phase, may be used to normalize affinity with respect to lipophilicity.

Keywords: covalent inhibitor, cruzain, cysteine protease, group efficiency, lipophilic efficiency, non-additivity, structure-activity relationship

1. Introduction

Chagas disease [1-3], also known as American trypanosomiasis, is caused by *T. cruzi* parasite infection and is a significant public health problem both in Latin America and internationally [4]. Cruzipain, the major *T. cruzi* cysteine protease, is expressed in all stages of the life-cycle of the parasite and is considered to be an attractive target for therapeutic intervention in the treatment of Chagas disease [5-7]. Enzyme inhibition studies typically make use of recombinant cruzain (Cz) which consists of the catalytic domain of cruzipain. Cruzain inhibitors have shown antichagasic activity in murine disease models [7, 8].

A commonly employed tactic in design of cysteine protease inhibitors is to incorporate an electrophilic entity, commonly referred to as a “warhead”, in the inhibitor structure [9, 10]. This enables a covalent bond to be formed between an electrophilic atom of the inhibitor and the thiol of the catalytic cysteine. Michael acceptors such as the vinylsulfone K777 [7] are typically irreversible inhibitors of cysteine proteases. A nitrile group in an inhibitor structure can form a covalent thioimidate adduct with the catalytic cysteine thiol and addition is typically reversible [11, 12]. Nitrile-based cruzain inhibitors have been reported [13-15] and *in vivo* activity in a murine disease model has been published [8] for inhibitors based on this warhead. Anti-trypanosomal activity has also been observed for nitrile-based cysteine protease inhibitors

in cell-based assays at concentrations below their cruzain K_i values, suggesting that inhibition of cysteine proteases other than cruzipain may be responsible for these effects [16].

A published [13] series of nitrile-based cruzain inhibitors that are structurally related to the cathepsin K inhibitor odanacatib [17] provided the starting point for this study. The compounds in this series typically feature a substituted biphenyl group at P3. The principal objective of the study was to establish a structure-activity relationship (SAR) for cruzain inhibition by deconstruction of the published inhibitor structures. Secondary objectives were to explore the utility of chromatographically measured $\log K_w$ for normalization of cruzain inhibition with respect to lipophilicity and to assess the anti-trypanosomal activity of the compounds against an intracellular form of the of *T. cruzi* Y strain.

2. Results

2.1 Synthetic chemistry

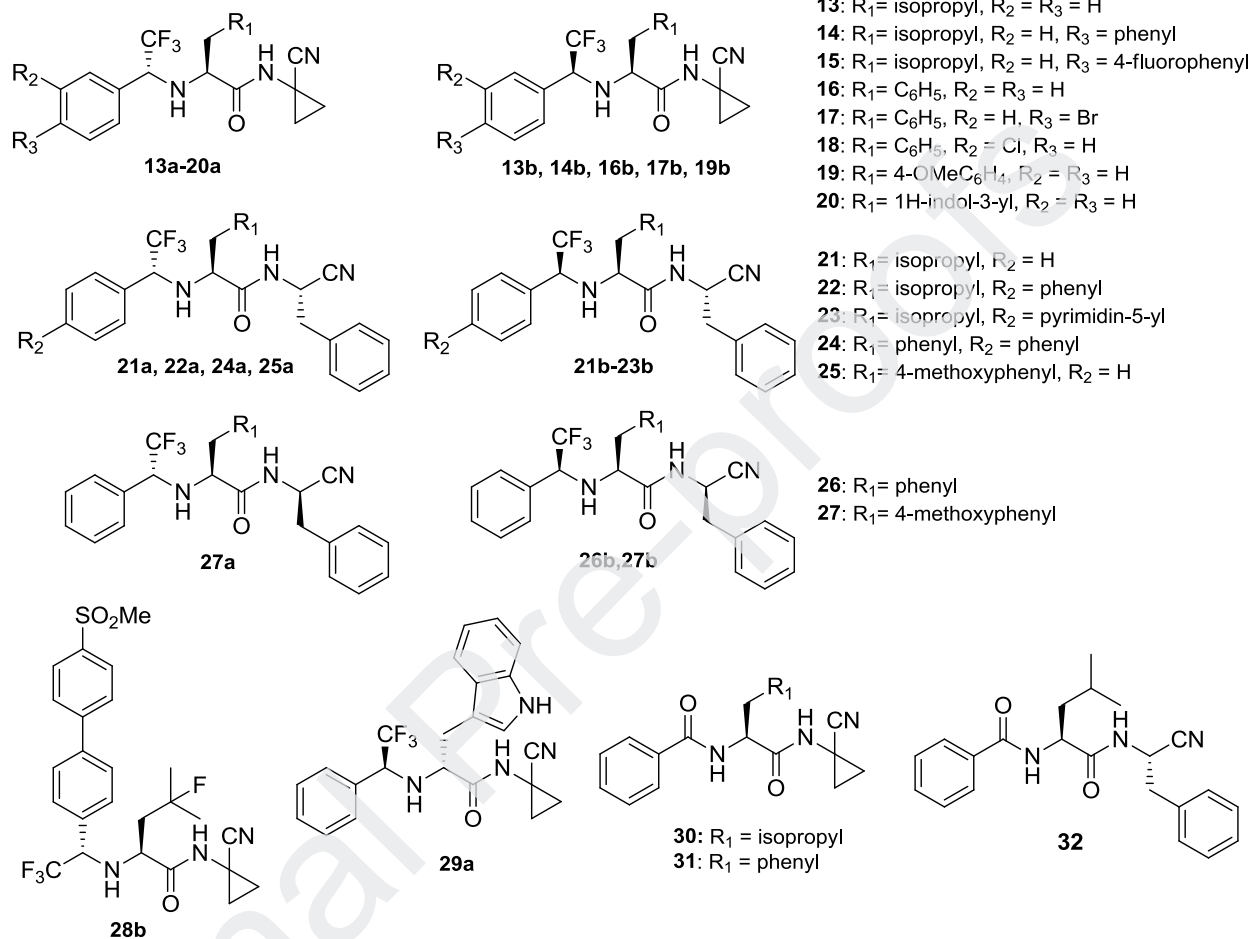
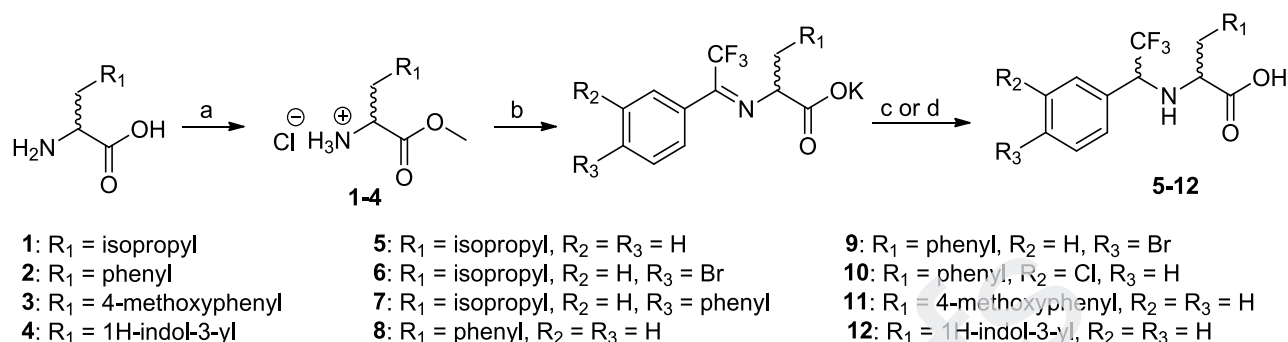


Chart 1. Compounds described in the present study

Structures of the compounds synthesized for elucidation of the SAR are shown in Chart 1. The syntheses of the intermediate amino acids, to be used in the peptide coupling, were carried out as shown in Scheme 1. Methyl esters (**1-4**) were produced from the commercial *D*- or *L*-amino acids, using thionyl chloride in dry methanol, following the procedure previously described [16]. After 18 h, the thin layer chromatography (TLC) indicated the total consumption of the starting material in all the cases. The following step consisted of preparation of the 2,2,2-

trifluorophenyl amino acid intermediates (**5-12**), as previously described with slight modification [18].



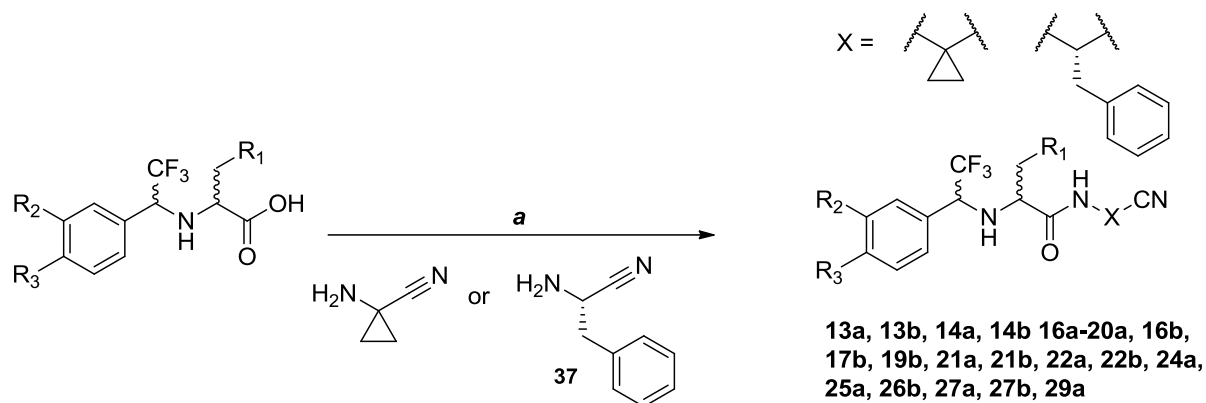
Scheme 1. Reagents and conditions: (a) SOCl₂, CH₃OH, reflux, 1 hr → r.t., overnight; (b) ArC(=O)CF₃, K₂CO₃, CH₃OH, 50 °C, 18 hrs; (c) 1M Zn(BH₄)₂ in DME, CH₃CN/CH₃OH (5:1), -40/-45 °C, 3 hrs; (d) NaBH₄, THF, r.t., 6 hrs.

Briefly, the amino esters (**1-4**) were reacted with the appropriate 2,2,2-trifluoroacetophenone, in the presence of potassium carbonate and methanol at 50 °C for 18 h, to afford the respective imines. The presence of water, resulting from imine formation, in the basic reaction medium at elevated temperature favors the hydrolysis of the methyl ester group, providing the potassium salts of the 2,2,2-trifluorophenyl imines. Due to their instability, all imines were used in the next step (for the diastereoselective reduction) without purification. As described by Hughes *et al.* [18], the reduction with NaBH₄ afforded, for the *L*-amino acid derivatives, the *R,S* diastereoisomers (*anti* isomers), reflecting the fact that the *re* face is sterically more hindered than the *si* face for the more stable conformation of these salts. This is due to the presence of the R₁ group of the *L*-amino acid moiety (phenyl, aryl, isopropyl), allowing the attack of the hydride ion to be, preferably, on the *si* side of the imine [18]. On the contrary, to obtain the *S,S* diastereoisomers (*syn* isomers) the imines were reduced with Zn(BH₄)₂. In that case, the formation of the *syn* isomer as a major diastereoisomer can be

explained by complexation of Zn^{2+} with the nitrogen and oxygen atoms at the 1,3-positions of the imine, respectively, making the *si* face sterically more hindered. When the starting material is the *D*-amino acid, the reduction of the corresponding imine gives the *S,R* diastereoisomer (*anti* isomer) with NaBH_4 and the *R,R* diastereoisomer (*syn* isomer) with $\text{Zn}(\text{BH}_4)_2$.

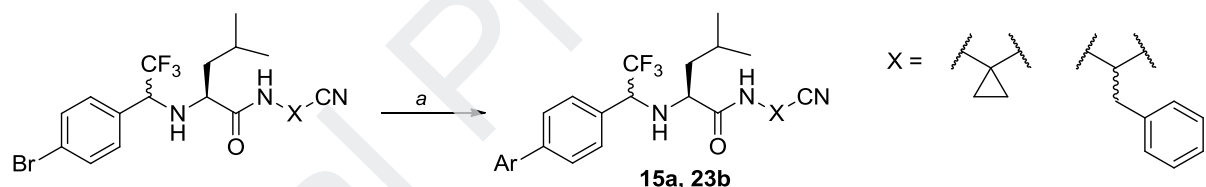
In general, we observed that NaBH_4 reduction of the imine produced the desired amines with a diastereomeric excess over 95%, while when using $\text{Zn}(\text{BH}_4)_2$ the diastereomeric excess was lower than 80%. The diastereomeric excesses in favor of the *syn* or *anti* isomer were measured by HPLC of the final compounds (**13-29**). If necessary, final products were purified by HPLC, equipped with a chiral column, to afford the desired product with *d.e.* > 99% and *e.e.* > 99%. In order to confirm the absence of epimerization in the chiral center of the amino acids during the synthetic steps, phenylalanine was employed as a model in this study. Therefore, racemic phenylalanine was used as a starting material, and the final compounds, after reduction (with NaBH_4 or $\text{Zn}(\text{BH}_4)_2$) and amine coupling, were analyzed by HPLC. The chromatograms of the racemic product were compared with those of **16a** and **16b** that came from the enantiopure phenylalanine (see SI), confirming the integrity of the stereogenic center with an enantiomeric excess > 99%.

After imine reduction the amino acids **5-12** were coupled with the appropriate amine, using HATU as the coupling agent, to afford **13, 14, 16-22, 24-27, 29** in good yield (Scheme 2). All compounds were fully characterized (characterization data for **16a** and **19a** are reported elsewhere [16]). The synthesis of 2-amino-3-phenylpropanenitrile (**37**), employed in the coupling to provide compounds **21-27, 32**, was carried out from *L*- or *D*-phenylalanine by two methods (see SI). Both methods gave the Boc-derivatives with a high enantiomeric excess (> 99% e.e.), as resulted from the HPLC analysis (see SI). Then, Boc removal was performed under a mild condition, using HCOOH .



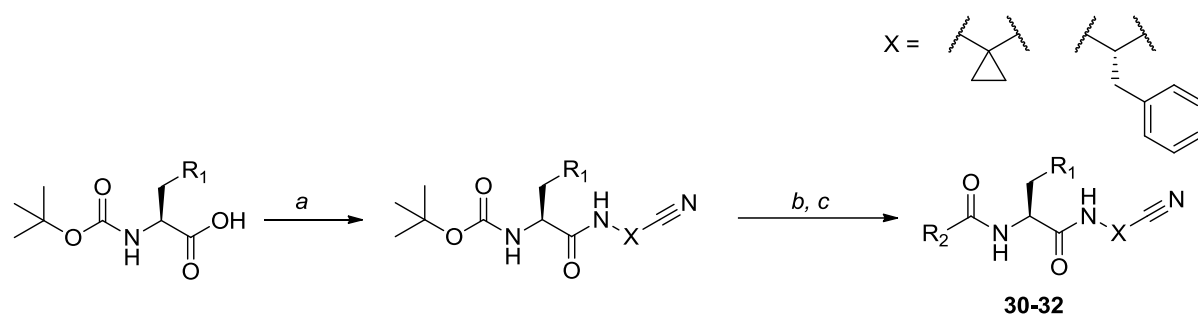
Scheme 2. Reagents and conditions: (a) HATU, DIPEA, H₂NXCN, r.t., 22hrs

Finally, compounds **15a** and **23b** were obtained by a Suzuki cross-coupling reaction of the aryl bromide intermediates (Scheme 3). According to the procedure described by Chen *et al.* [19], the bromides reacted in the presence of sodium carbonate, with the appropriate boronic acid pinacol ester, using PdCl₂dppf as catalyst, in DMF, at 80°C for 3hrs (Scheme 3).



Scheme 3. Reagents and conditions: (a) ArB(OH)₂ pinacol ester, PdCl₂dppf, DMF, 80°C, 3 hrs, argon atmosphere.

Compounds **30-32** were prepared following the general procedure showed in Scheme 4. The Boc-*L*-amino acid was coupled with the selected amine by HATU, followed by Boc removal in a mild condition (HCOOH). Next, the free amino group was coupled with benzoic acid using HATU as the coupling agent. This procedure gave the final compound with an *e.e.* > 99 %. All compounds were fully characterized (characterization data for **31** is reported elsewhere [14]).



Scheme 4. *Reagents and conditions:* (a) H_2NXCN , HATU, DIPEA, DMF, 16 hrs, r.t., argon atm.; (b) HCOOH , 16 hrs, r.t.; (c) $\text{R}_2\text{CO}_2\text{H}$ acid, HATU, DIPEA, DMF, 16 hrs, r.t., argon atm.

2. 2 Enzyme inhibition and lipophilicity

Measured pK_i values for inhibition of cruzain and cathepsin L and lipophilicity measurements performed by HPLC using an immobilized artificial membrane column are given in Table 1 for the compounds in Chart 1. The most potent compound (**22b**; $\text{pK}_i = 9.2$) synthesized during the course of the current study is the des-methylsulfonyl analog of a cruzain inhibitor for which a pIC_{50} value of 9.7 has been reported [13].

Table 1. Enzyme inhibition and lipophilicity

Compound	Cz pK _i ^{a,b}	SE Cz pK _i ^{a,c}	CatL pK _i ^{a,d}	SE CatL pK _i ^{a,e}	logK _w ^f	SE logK _w ^g
13a	6.7	0.01			1.1	0.02
13b	7.4	0.01				
14a	7.2	0.01	6.2	0.03	2.8	0.01
14b	8.1	0.01	6.1	0.03	2.6	0.01
15a	7.1	0.02	6.0	0.03	2.8	0.02
16a	5.6	0.07			1.4	0.02
16b	6.0	0.01	6.8	0.05	1	0.004
17b	5.7	0.04	6.6	0.02	1.7	0.02
18a	5.5	0.05			1.7	0.02
19a	5.1	0.05			1.5	0.03
19b	5.4	0.05			1.4	0.02
20a	< 5		6	0.03		
21a	6.4	0.02	6.6	0.02	2.2	0.02
21b	8.8	0.01	8.3	0.03	2.3	0.02
22a	6.6	0.02			3.1	0.2
22b	9.2	0.01	5.8	0.03	3.2	0.2
23b	8.8	0.01	7.6	0.01		
24a	< 5					
25a	5.4	0.05	5.8	0.07	2.7	0.01
26b	5.6	0.03	6.2	0.05	2.6	0.02
27a	< 5		< 5			
27b	6.4	0.02	6.2	0.01	2.7	0.02
28b	6.9	0.09	5.9	0.04	2	0.01
29a	< 5		5.9	0.03		
30	7.3	0.01	7.7	0.02		
31	6.5	0.02	7.4	0.03	0.76	0.01
32	7.3	0.02	7.2	0.04		

^a pK_i = -log₁₀(K_i/M)^b Cruzain pK_i^c Standard error in cruzain pK_i^d Cathepsin L pK_i^e Standard error in cathepsin L pK_i^f logK_w determined by HPLC using IAM stationary phase^g Standard error in logK_w

2.3 Anti-trypanosomal assay results

Only two of the compounds listed in Table 1 exhibited concentration-responsive activity against intracellular *T. cruzi* amastigotes infecting human U2OS cells [20-22]. EC₅₀ and CC₅₀ values of 11 (± 1) μM and 33 (± 5) μM respectively were determined for **20a**. Compound **29a** was less potent (EC₅₀/μM = 26 ± 0.3) and CC₅₀ could not be determined for this compound.

Benznidazole presented potency and efficacy values corresponding to data previously reported for Y strain [20].

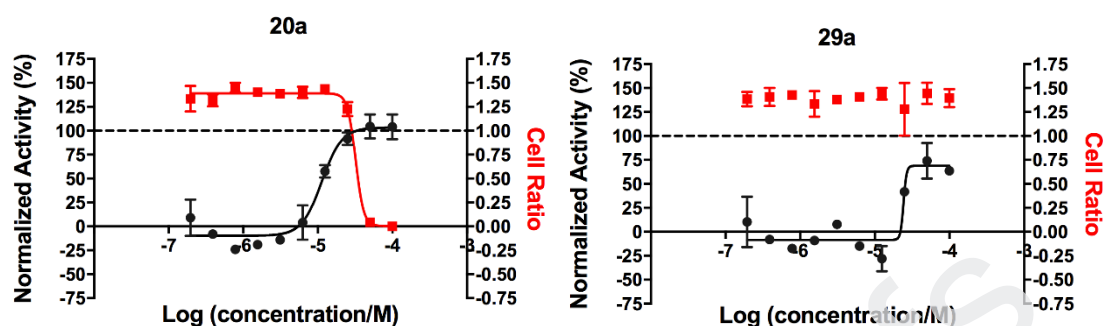


Figure 1. Concentration-response curves for compounds and reference compound benznidazole after 96 h of exposure to U2OS cells infected with *Trypanosoma cruzi* Y strain. Data points are means and error bars represent standard deviations of two replicates. Black dots and curves represent data of compound activity whereas red dots and curves indicate the cell ratio parameter.

3. Discussion





3.1 Structure-activity relationships

The principal objective of this study is to deconstruct published trifluoroethylamine-based cruzain inhibitors to structures of lower molecular complexity [23] in order to establish a structure-activity relationship (SAR). In medicinal chemistry, SARs are typically specified in terms of the effects of structural transformations (e.g., substitute chlorine for hydrogen) on potency or affinity. In this study, we use $[X \rightarrow Y]$ to specify structural transformations where the labels X and Y can be defined flexibly by the user to refer to structure number, substructure (e.g. P3-phenyl), functional group (e.g. aldehyde), or configuration as required [10]. The affinity difference, ΔpK_i , corresponding to the $[X \rightarrow Y]$ transformation can be written as:

$$\Delta pK_i[X \rightarrow Y] = \Delta pK_i[Y] - \Delta pK_i[X] \quad (1)$$

The basis of the lead-likeness [24] concept is that optimization of leads typically results in increased lipophilicity and molecular size and these parameters may be regarded as the primary physicochemical risk factors in drug design [25]. The structural modifications for which the largest increases in affinity are accompanied by the smallest increases in risk can be regarded being the most efficient in the context of hit or lead optimization [25]. This is the basis of group efficiency (GE) [26] and a highly efficient structural transformation can also be seen as a type of activity cliff [27, 28]. Although GE [26] is frequently presented [29] as a substituent property, it is actually structural transformations with which values of the GE metric should be associated [25]. One limitation of GE as a tool for SAR analysis is that it is not defined for structural transformations such as inversion of configuration, aza-substitution and amide reversal for which there is no net change in the number of non-hydrogen atoms. The effects of inverting chiral centers are of considerable interest [30, 31] since the effects on logP are typically small (zero in the case of compound with a single chiral center in its molecular structure). The substructural transformations that form the basis for the analyses in this study are given in Table 2.

Table 2. Key for structural transformations depicted in Figures 2 and 3

Label	Transformation	ΔN_{NH} ^a	Representation in Figure 2	Representation in Figure 3
A	[P1-cyclopropyl → P1-benzyl(S)]	5		
B	[P3-phenyl → P3-biphenyl]	6		
C	[P3-S → P3-R]	0	N/A ^b	
D	[P2-Leu → P2-Phe]	3		N/A ^b

^a Change in number of non-hydrogen atoms

^b Not applicable

The published [13] cruzain inhibitors were deconstructed to the structural prototype **13b** by truncation of P3 biphenyl substituent to phenyl and by replacement of the benzyl substituted P1 linker with cyclopropane. Compound **13a**, in which the P3 chiral center of **13b** is *S* rather than *R*, and the dipeptide nitrile **30** were also used as structural references. The effects of

synthetic elaboration are summarized by plotting pK_i versus the change (ΔN_{nH}) in the number of non-hydrogen atoms relative to the reference structure (Figure 2). Plotting against ΔN_{nH} rather than N_{nH} allows the dipeptide nitrile SAR to be visualized in the same frame of reference as the other inhibitors. The gradient of the line linking two points quantifies the sensitivity of affinity to an increase in molecular size [25]. For a structural transformation associated with a net change in molecular size, the extent to which the different lines representing the structural transformation are parallel gives a visual indication of the degree to which SAR is additive.

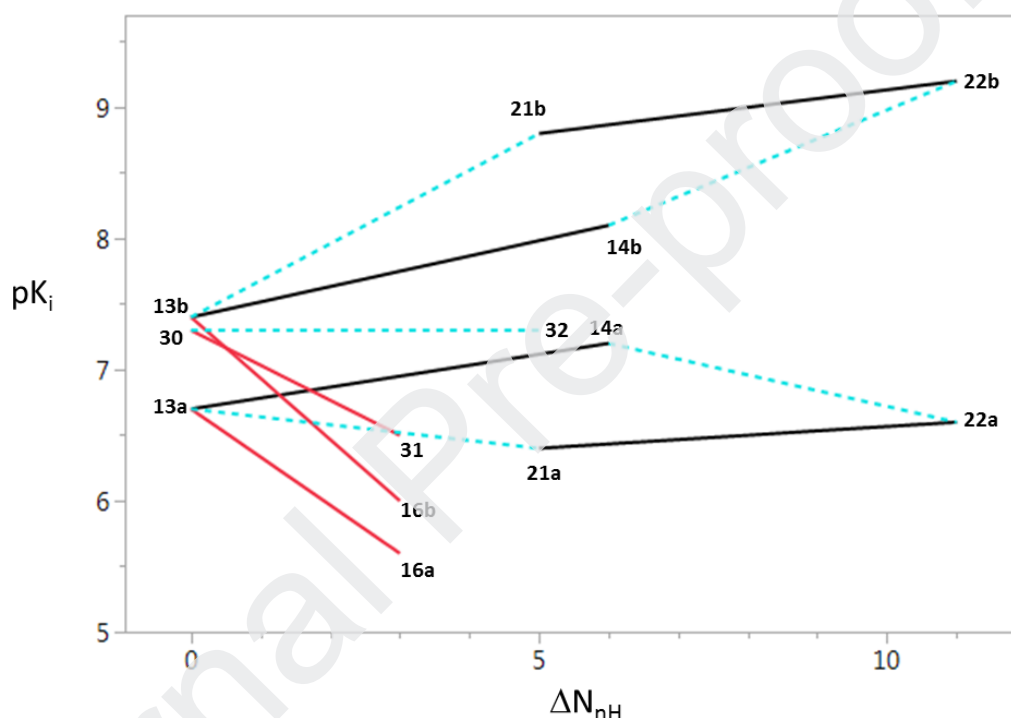


Figure 2. Sensitivity of cruzain pK_i to structural modifications A, B and D (see Table 2 for key)

The [phenyl \rightarrow biphenyl] transformation at P3 (solid black line) leads to increases in pK_i for trifluoroethylamines regardless of the configuration of the P3 substituent. In contrast, the [cyclopropane \rightarrow benzylmethylene] transformation at P1 (dashed blue line) leads to an increase in pK_i when the P3 configuration is *S* but a decrease in pK_i where this is *R*. The [cyclopropane

→ benzylmethylene] transformation at P1 (dashed blue line) has no effect the affinity of the dipeptide nitrile **30**. Exchange of the P2 leucine for phenylalanine (solid red line) leads to decreases in affinity ranging from 0.7 to 1.4 for the three reference compounds.

Substitution of the P3 substituents with a halogen typically leads to small decreases in affinity and the pK_i values for **15a**, **17b** and **18a** are all within 0.3 log units of the respective values for the compounds from which they were derived. Aza-substitution of the P3-biphenyl is well tolerated and **23b** is only 0.4 log units less potent than **22b**. Replacement of the P2 phenylalanine by O-methyltyrosine for **16a** and **16b** resulted in decreases in pK_i of 0.5 and 0.6 respectively. In contrast, the [**26b** → **27b**] transformation leads to an increase in pK_i of 0.8 log units which illustrates how the P1-substituent can influence the P2-substituent SAR. Compound **25a** was observed to be at least 0.4 log units more potent than **27a** and this preference for the *S* configuration at P1 is consistent with what has been reported [13] for analogues substituted with 2-fluoro-4-cyanobenzyl at P1.

Additivity [32-35] is an essential concept in interpretation of SAR and additivity is assumed when performing Free-Wilson analysis [36]. For the example of two hydrogen atoms on a scaffold being substituted with groups X and Y, the requirement for additivity can be written as:

$$\Delta pK_i[HH \rightarrow XY] = \Delta pK_i[HH \rightarrow XH] + \Delta pK_i[HH \rightarrow HY] \quad (2)$$

Although additivity of SAR is usually discussed in terms of adding substituents, the concept can be applied to any structural transformation (e.g., inversion of configuration) and the labels 0 or 1 can be used more generally to indicate whether or not a structural transformation has been applied. Additivity can also be quantified for physicochemical properties, such as solubility, permeability, partition coefficient and reactivity, provided that differences in values of the relevant measurable quantities are physically meaningful. The degree of additivity can

be quantified for a pair of structural transformations by δ which is defined for a biochemical, biophysical or physicochemical property, X, by:

$$\delta[00 \rightarrow 11] = \Delta X[00 \rightarrow 11] - (\Delta X[00 \rightarrow 10] + \Delta X[00 \rightarrow 01]) \quad (3)$$

The effects of applying two structural transformations can be classified as additive ($\delta = 0$), subadditive ($\delta < 0$) or superadditive ($\delta > 0$). In analysis of non-additivity, structural transformations are typically defined so that their application leads to increased molecular complexity and inversion of configuration would typically be regarded as having no effect on molecular complexity. Subadditive SAR should generally be anticipated for structural changes that lead to an increase in molecular complexity [23], especially if there is a high degree of constraint in the system [25]. Factors such as conformational rigidity, covalent protein-ligand contact and multiple hydrogen bonds between protein and ligand would all be expected to increase the degree of constraint. Non-additive SAR is particularly valuable for testing and validation of models for binding affinity of ligands [37].

The cruzain inhibition SAR associated with structural transformations A, B and C (defined in Table 2) is illustrated in Figure 3. Opposite faces of the cube shown in Figure 3 represent the application of the two structural transformations to starting points that are connected by the third structural transformation. The difference between ΔpK_i values associated with parallel sides of each cube face quantifies the extent to which the associated SAR is non-additive while the dependence of the ΔpK_i values on the order in which structural transformations are applied indicates whether the SAR is subadditive or superadditive. This can be illustrated by the effects of applying structural transforms A and C to **13a** (see front face of the cube in Figure 3). The difference ($\delta = 1.7$) between the of ΔpK_i value resulting from simultaneous application of both structural transformations and the sum of ΔpK_i values corresponding to the individual structural transformations shows that the associated SAR is strongly non-additive. In each case, the ΔpK_i

value for a structural transformation is greater when it is the second to be applied than if it is applied first which indicates that the SAR is superadditive for this pair of structural transformations.

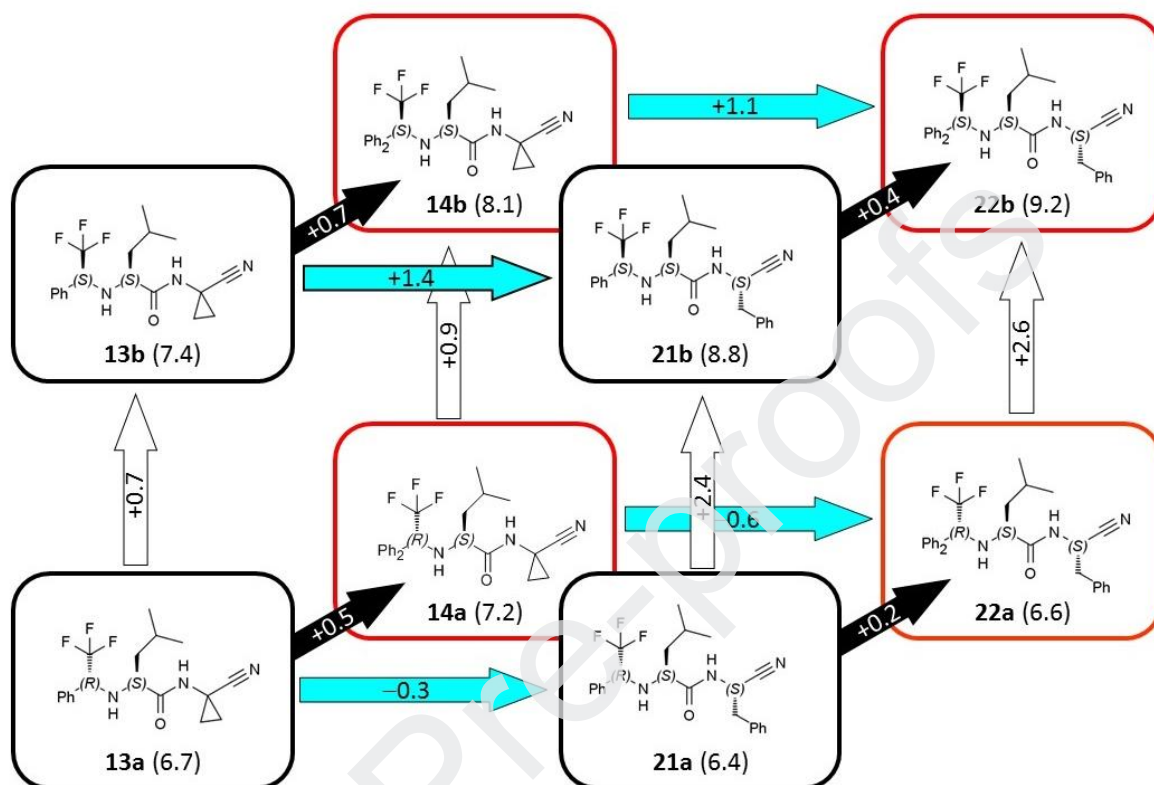


Figure 3. Non-additivity in SAR for structural transformations A, B and C (see Table 2 for key; Ph = phenyl; Ph₂ = 4-biphenyl)

The non-additivity in the SAR depicted in Figure 3 is summarized in Table 3. One interpretation of the superadditive SAR observed for the A and C transformations is that having the P3 substituent with the *S* configuration enables the P1 benzyl substituent to interact more effectively with the protein than would be the case for the *R* configuration. Nevertheless, caution is needed when interpreting non-additivity in terms of molecular interactions because the phenomenon is inherently non-local in nature.

Table 3. Non-additivity in SAR for structural transformations A, B and C (see Table 2 for key)

Initial structure	Transformations ^a		$\Delta pK_i[00 \rightarrow 10]$ ^b	$\Delta pK_i[00 \rightarrow 01]$ ^b	$\Delta pK_i[00 \rightarrow 11]$ ^b	δ ^b
13a	A	B	-0.3	+0.5	-0.1	-0.3
13b	A	B	+1.4	+0.7	+1.8	-0.3
13a	A	C	-0.3	+0.7	+2.1	+1.7
14a	A	C	-0.6	+0.9	+2.0	+1.7
13a	B	C	+0.5	+0.9	+1.4	0
21a	B	C	+0.2	+2.4	+2.8	+0.2

^a Defined in Table 2

^b Defined in equation (3)

3.2 Cruzain versus cathepsin L selectivity

Compound **22b** shows significant selectivity for cruzain over cathepsin L and the pK_i values for inhibition of these cysteine proteases differ by 3.4 log units. This is consistent with what has been reported for structural analogs of this compound [13]. The corresponding pK_i differences (cruzain – cathepsin L) for compounds **14b** (2.0) and **21b** (0.5) show that both the P3 biphenyl and P1 benzyl influence selectivity. The P3 configuration also influences selectivity as exemplified by the pK_i differences (cruzain – cathepsin L) for **14a** (1.0) and **21a** (-0.2). Aza-substitution of the P3 biphenyl of **22b** leads to reduced selectivity as shown by the pK_i values of 8.8 (cruzain) and 7.6 (cathepsin L) measured for **23b**.

3.3 Normalization of affinity with respect to measured lipophilicity

Affinity can be normalized with respect to lipophilicity by subtracting logD [38] or logP [39] from pK_i and the resulting quantity is often referred to as ligand lipophilicity efficiency (LLE), lipophilic ligand efficiency (LLE) or lipophilic efficiency (LipE) [29]. It has been suggested [25, 40, 41] that it would be more appropriate to use the actual trend in the data for normalization and this can be done by first establishing a linear free energy relationship (LFER) [42] between pK_i and the relevant measure of lipophilicity. The slope of the LFER quantifies the sensitivity of affinity to an increase in lipophilicity and, in general, varies with both target and the scaffold on which the ligands are based [25]. The residuals (equation 4) from fitting

the LFER quantify the extent to which individual pK_i values beat (or are beaten by) the trend in the data [25, 40, 41]. This approach to normalization of affinity is analogous to that introduced in 1984 by Andrews *et al* [43].

$$pK_i[\text{resd}] = pK_i[\text{expt}] - pK_i[\text{pred}] \quad (4)$$

Scott and Waring have emphasized the benefits of using measured, rather than calculated, lipophilicity for normalization of affinity [44]. In our study, lipophilicity was measured using high performance liquid chromatography (HPLC) with an immobilized artificial membrane (IAM) column. This assay is typically used for permeability assessment and lipophilicity measured in this manner may also be described as phospholipophilicity. A plot of pK_i versus $\log K_w$ is shown in Figure 4A and the correlation between these quantities is weak ($R^2 = 0.27$; Table 4). Provided that it is not merely due to a narrow range in the data, a weak correlation between affinity and lipophilicity is actually desirable in optimization projects because it points to specific SAR rather than affinity being driven solely by lipophilicity [25]. The plot of $pK_i[\text{resd}]$ versus $\log K_w$ (Figure 4B) shows the binding of **21b** to be more efficient with respect to lipophilicity than that of the more potent **22b**. An advantage of presenting data in this manner is that the extent to which the affinity of a compound beats (or is beaten by) the trend in the data can be easily perceived.

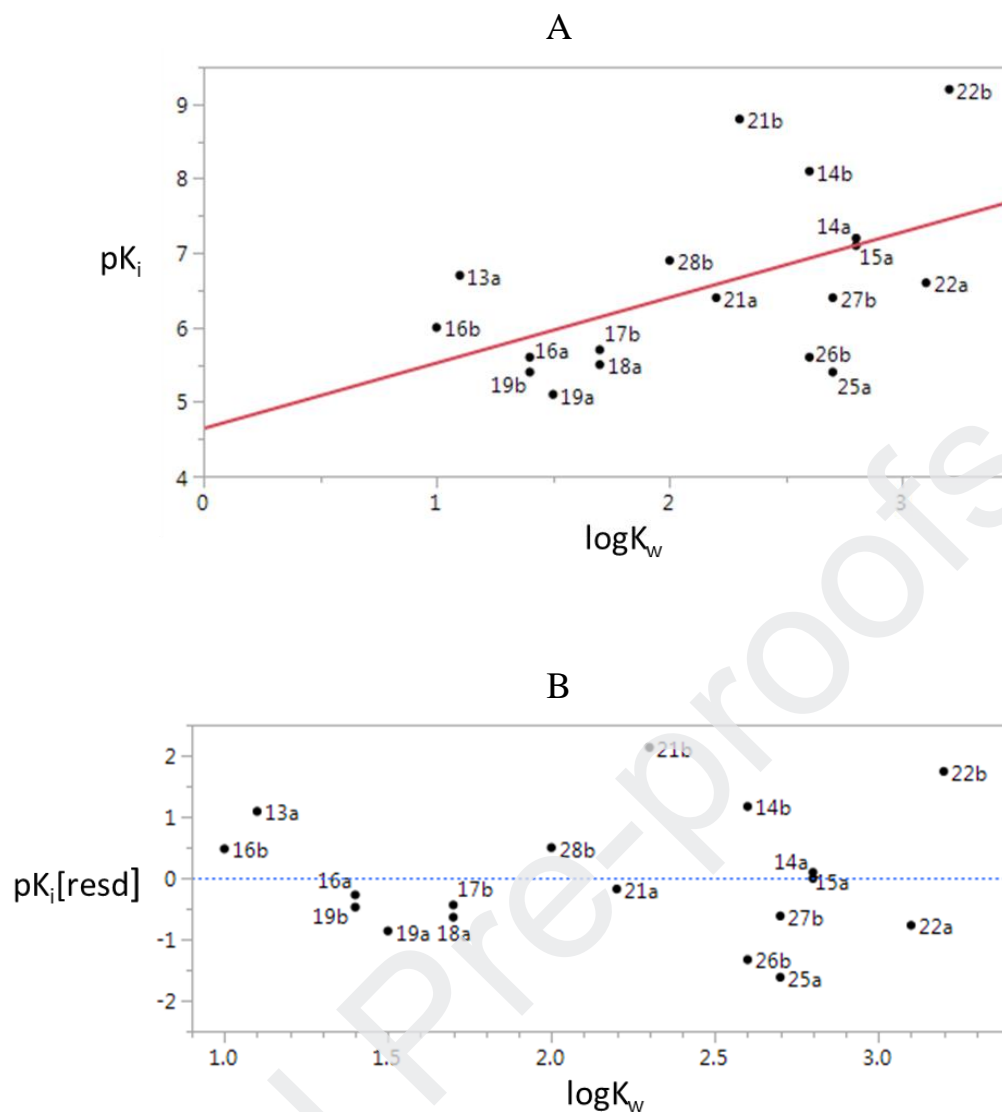


Figure 4. Normalization of affinity with respect to lipophilicity

Table 4. Relationship between pK_i and $\log K_w$

$pK_i = A_0 + (A_1 \times \log K_w)$						
N ^a	A_0	SE A_0 ^b	A_1	SE A_1 ^c	RMSE ^d	R^2 ^e
18	4.6	0.82	0.88	0.36	1.0	0.27

^a Number of observations

^b Standard error in A_0

^c Standard error in A_1

^d Root mean square error

^e Coefficient of determination

Small differences in $\log K_w$ were observed for diastereomers related by inversion of the configuration of the P3 substituent and these appear to be influenced by the nature of the P1 substituent (Table 5). Variation in $\Delta\log K_w$ values corresponding to a specific structural transformation can be regarded as non-additivity in the structure-property relationship.

Table 5. Differences in $\log K_w$ for diastereomers

Transformation	P1-group	$\Delta\log K_w$
[14a→14b]	Cyclopropane	-0.2
[16a→16b]	Cyclopropane	-0.4
[19a→19b]	Cyclopropane	-0.1
[21a→21b]	benzyl	+0.1
[22a→22b]	benzyl	+0.1

3.4 Anti-trypanosomal activity

Meaningful SAR cannot be derived for the cell-based assay results because it was only possible to measure EC_{50} values for **20a** (11 μM) and **29a** (26 μM). In general, failure of enzyme inhibitory activity to translate to activity in a cell-based assay should be anticipated, especially for an intracellular parasite, and may reflect poor permeability or an enzyme inhibition model that is not relevant in the cellular context [16]. An observation that compounds are more potent in a cell-based assay than in the corresponding enzyme inhibition assay is more significant (provided that it is not the result of non-specific cytotoxicity) and may indicate that the effects on the cells are due to engagement of targets other than the cellular equivalent of the enzyme used in the inhibition assay [16]. Although neither of the two compounds for which it was possible to measure EC_{50} shows significant cruzain inhibition ($pK_i < 5$), their potencies in the cell-based assay are too low to allow any inference to be drawn as to whether or not their effects in cells are due to inhibition of enzymes other than cruzipain.

4. Conclusion

We have deconstructed a published series of potent cruzain inhibitors and show that plotting affinity against molecular size allows features of the structure-activity relationship to be easily visualized. Examination of the structure-activity relationship reveals that the P3 biphenyl substituent can be truncated to phenyl with the loss of only 0.4 log units of affinity. In combination, the effects of inverting the configuration of the P3 substituent and substituting at P1 with benzyl were observed to be strongly non-additive. We also show how lipophilicity measured by HPLC with an immobilized artificial membrane can be used to normalize affinity.

5. Experimental Section

5.1 Synthetic chemistry

5.1.1 General materials and methods

Commercially available reagents and solvents were used as received, without further purification, unless otherwise stated. All solvents were dried and distilled before use by standard procedures. The reaction progress was monitored by thin-layer chromatography on silica gel (aluminum foils) and spotted under UV light (254 nm), followed by staining with ethanolic 5% phosphomolybdic acid solution or with aqueous KMnO_4 . Purification by column chromatography was carried out on silica gel (Merck 60, particle size 0.040 -0.063 mm). Melting points were determined on a Kofler apparatus. Infrared spectra were obtained using FTIR at 4.0 cm^{-1} resolution and are reported in wavenumbers. The analytical HPLC system consisted of a Shimadzu LC (Kyoto, Japan) equipped with an LC-20AT pump, an LC-20AD pump, a SIL-20A HT autosampler, a DGU-20A5 degasser, a CBM-20A, SPDM20A DAD detector and an FRC-10A fraction collector. In the established HPLC protocol, chiral analysis was carried out at $32 \text{ }^\circ\text{C}$ (column oven) where not otherwise specified. The most common mobile phase composition was acetonitrile-water (50:50) (v/v). Volumes of $10 \text{ }\mu\text{L}$ (analytical) and $1000 \text{ }\mu\text{L}$ (semipreparative) were injected. Quantification was carried out at 200–800 nm

and the chromatographic run time varied according to the sample. Data acquisition was performed using an LC solution software version 1.26 SP5. The LC system was coupled to an AmaZon SL ion trap mass spectrometer (Bruker Daltonics, Bremen, Germany) equipped with electrospray ionization (ESI) interface. Data acquisition was performed with Bruker Daltonics Data Analysis software (version 4.2.383.1). ^1H -NMR, ^{13}C -NMR and ^{19}F NMR spectra were recorded at 400 or 500, 100 and 376 MHz respectively in CDCl_3 or $\text{DMSO-}d_6$ at 25°C , in a Varian Mercury 400 or Bruker Avance DRX 500. Chemical shifts (δ) were reported in ppm and the coupling constants (J) in Hertz (Hz). ^1H -NMR spectra were referenced to DMSO ($\delta = 2.54$ ppm) or CHCl_3 ($\delta = 7.26$ ppm) as internal standard, and ^{13}C -NMR were referenced to the central signal of the $\text{DMSO-}d_6$ multiplet ($\delta = 40.45$ ppm) or CDCl_3 triplet ($\delta = 77.00$ ppm). Signal multiplicity was assigned as singlet (s), doublet (d), double doublet (dd), triplet (t), double triplet (dt), quartet (q), quintuplet (qt), multiplet (m) and broad (br). The high-resolution mass spectra (HRMS) were recorded using a Q-TOF Micromass equipment (Waters, UK) employing ESI-MS techniques.

General Procedure for the synthesis of trifluoramino acids 9-12

To a solution of aminoester hydrochloride **1-4** (2.21 mmol) in dry methanol (5 mL), under an argon atmosphere, potassium carbonate (4.42 mmol) and the appropriate trifluoroacetophenone (2.43 mmol) were added. The mixture was stirred at 50°C for 18 h and then, the reaction was cooled to r.t., filtered and the solvent was removed under *vacuum*. The collected oil was used in the next step without further purification.

Reduction with $\text{Zn}(\text{BH}_4)_2$: To a solution of imine/potassium carboxylate (2.21 mmol) in CH_3CN (15 mL) and MeOH (1.5 mL), a freshly prepared solution of $\text{Zn}(\text{BH}_4)_2$ in DME (1 mmol/mL, 1.5 mL) was added at $-40/-45^\circ\text{C}$. After 3 hrs at $-40/-45^\circ\text{C}$, the reaction mixture was allowed to warm until 0°C and 1N HCl was added until pH 2-3. The aqueous mixture was extracted

with EtOAc (3x 25mL); the combined organic phases were dried on Na₂SO₄, evaporated under vacuum and purified by flash column chromatography (AcOEt: *n*-Hexane 30:70 v/v) to give the acid in a good yield (50-70%).

Reduction with NaBH₄: The imine/potassium carboxylate (2.21 mmol) was suspended in dry THF (25 mL) and MeOH (1.5 mL), stirred at 0°C and then, NaBH₄ (12.15 mmol) was added in only batch. After stirring for 6 hrs, at room temperature, the system was cooled to 0°C and quenched with 2 M HCl solution until stopping the gas release (final pH 2-3). Next, the organic solvent was evaporated under vacuum and the crude extracted with ethyl acetate (3 x 10 mL). The combined organic layers were then dried over Na₂SO₄, filtered, and evaporated in rotary evaporator. Purification by flash column chromatography (AcOEt: *n*-Hexane 30:70 v/v) afforded the trifluoroamino acid (56-71% yield).

General Procedure for the synthesis of dipeptidyl nitriles 13, 14, 16-22, 24-27, 29

The appropriate acid (0.82 mmol), HATU (1.22 mmol, 465 mg) and amine as hydrochloride salt or a free base (0.90 mmol) were sequentially introduced into a 25 mL round bottomed flask, provided with a magnetic stirrer and under argon atmosphere. Next, dry DMF (13 mL) and *N,N*-diisopropylethylamine (2.05 mmol.) were added into the flask. The reaction was stirred at room temperature overnight. Ethyl acetate (100 mL) was added to the reaction mixture and the organic layer was washed with saturated aqueous NaHCO₃ (3x), NH₄Cl (3x) and NaCl solution (3x). The organic layer was then dried over Na₂SO₄, filtered, and evaporated in rotary evaporator. Purification by flash column chromatography (AcOEt: *n*-hexane) afforded the dipeptidyl nitriles. When necessary, compounds were purified by HPLC equipped with a chiral column.

5.1.1 (S)-N-(1-cyanocyclopropyl)-4-methyl-2-(((R)-2,2,2-trifluoro-1-phenylethyl)amino)pentanamide (**13a**)

Silica/ AcOEt: *n*-hexane 30:70 *v/v* (71% yield). Colorless oil. $[\alpha]_D^{24} = -108.74^\circ$ (MeOH, $c = 1.03 \times 10^{-3}$). FT-IR (KBr, cm^{-1}): 3319, 2959, 2253, 1686, 1525, 1331, 1263, 1173, 1107, 887, 704. ^1H NMR (400 MHz, CDCl_3): δ 7.66 (s, 1H), 7.45-7.39 (m, 3H), 7.33-7.31 (m, 2H), 3.80 (q, $J = 7.37$ Hz, 1H), 3.07 (dd, $J = 3.64$ and 9.77 Hz, 1H), 1.99 (s, 1H), 1.64-1.42 (m, 5H), 1.41-1.35 (m, 1H), 1.24-1.19 (m, 2H), 0.85 (d, $J = 6.28$ Hz, 3H), 0.57 (d, $J = 7.17$ Hz, 3H). ^{13}C NMR (100 MHz, CDCl_3): δ 174.8, 133.3, 129.6, 129.1, 128.0, 124.9 (q, $J = 230$ Hz), 119.8, 63.8 (q, $J = 30$ Hz), 59.0, 42.6, 24.6, 23.2, 23.1, 20.9, 20.1, 16.9, 16.4. HRMS (ESI): m/z calcd for $\text{C}_{18}\text{H}_{23}\text{F}_3\text{N}_3\text{O}$ $[\text{M}+\text{H}]^+$: 354.17877; found: 354.17926. HPLC: Lux® 5 μm Cellulose-2, 250 x 4.6 mm, Acetonitrile/Water: 50:50, 0.5mL min^{-1} , t_r : 13.888 min, 206nm. CHIRALPAK® IC-5 (5 μM), 250 x 4.6 mm, Acetonitrile/Water: 50:50, 0.5mL min^{-1} , t_r : 20.850 min, 206nm.

After HPLC purification *d.e.* = 96.0 %.

5.1.2 (S)-N-(1-cyanocyclopropyl)-4-methyl-2-(((S)-2,2,2-trifluoro-1-phenylethyl)amino)pentanamide (**13b**)

Silica/ AcOEt: *n*-hexane 30:70 *v/v* (71% yield). White solid. M.p. 144-146 °C. $[\alpha]_D^{24} = +8.00^\circ$ (MeOH, $c = 1.02 \times 10^{-3}$). FT-IR (KBr, cm^{-1}): 3319, 2959, 2253, 1686, 1525, 1331, 1263, 1173, 1107, 887, 704. ^1H NMR (400 MHz, CDCl_3): δ 7.42-7.37 (m, 3H), 7.34-7.32 (m, 2H), 7.15 (s, 1H), 4.03 (q, $J = 7.37$ Hz, 1H), 3.35 (dd, $J = 4.75$ and 8.95 Hz, 1H), 2.12 (s, 1H), 1.76 (ddq, $J = 6.53$, 8.74 and 13.00 Hz, 1H), 1.60 (ddd, $J = 4.78$, 8.81 and 13.70 Hz, 1H), 1.49-1.36 (m, 3H), 1.00-0.96 (m, 1H), 0.95 (d, $J = 2.50$ Hz, 3H), 0.94 (d, $J = 2.56$ Hz, 3H), 0.83-0.77 (m, 1H). ^{13}C NMR (100 MHz, CDCl_3): δ 174.8, 134.1, 129.5, 129.0, 125.3 (q, $J = 220$ Hz), 119.6, 64.2, 63.8 (q, $J = 28.7$ Hz), 42.6, 24.8, 23.1, 21.7, 19.9, 16.8, 16.2. HRMS (ESI): m/z calcd for

$C_{18}H_{23}F_3N_3O$ $[M+H]^+$: 354.17877; found: 354.17926. HPLC: Lux® 5 μ m Cellulose-2, 250 x 4.6 mm, Acetonitrile/Water: 50:50, 0.5 mL min⁻¹, t_R : 12.912 min, 206nm. After HPLC purification *d.e.* > 99%.

5.1.3 (S)-2-(((R)-1-([1,1'-biphenyl]-4-yl)-2,2,2-trifluoroethyl)amino)-N-(1-cyanocyclopropyl)-4-methylpentanamide (**14a**)

Silica/ AcOEt: *n*-hexane 30:70 v/v (78% yield). White solid, Mp 149-151°C. $[\alpha]_D^{24} = -126^\circ$ (MeOH, $c = 1.21 \times 10^{-3}$). FT-IR (KBr, ν_{max}): 3323, 2958, 2245, 1683, 1519, 1267, 1172, 1103, 894, 765, 696 cm⁻¹. ¹H NMR (400 MHz, CDCl₃): $\delta = 7.63$ -7.66 (m, 3H), 7.59-7.61 (m, 2H), 7.45-7.49 (m, 2H), 7.37-7.42 (m, 3H), 3.88 (m, 1H), 3.12 (dd, $J = 2.9$ e 9.6 Hz, 1H), 1.50-1.64 (m, 4H), 1.40-1.44 (m, 1H), 1.21-1.32 (m, 3H), 0.88 (d, $J = 5.9$ Hz, 3H), 0.61 (d, $J = 6.0$ Hz, 3H) ppm. ¹³C NMR (100 MHz, CDCl₃): $\delta = 174.9$, 142.6, 140.0, 132.1, 128.9, 128.5, 127.8, 127.7, 127.1, 125.0 (q, $J = 220$ Hz), 119.8, 63.5 (q, $J = 29.3$ Hz), 59.0, 42.7, 24.7, 23.2, 21.0, 20.1, 16.9, 16.4 ppm. HRMS (ESD): m/z calcd for $C_{24}H_{27}F_3N_3O$ $[M + H]^+$: 430.21007; found: 430.21014. HPLC: Lux® 5 μ m Cellulose-2, 250 x 4.6 mm, Acetonitrile/Water: 55:45, 0.5 mL min⁻¹, t_R : 17.631 min, 206nm. After HPLC purification *d.e.* > 99%.

5.1.4 (S)-2-(((S)-1-([1,1'-biphenyl]-4-yl)-2,2,2-trifluoroethyl)amino)-N-(1-cyanocyclopropyl)-4-methylpentanamide (**14b**)

Silica/ AcOEt: *n*-hexane 10:90 to 30:70 v/v (78% yield). White solid. M.p. 200- 204°C. $[\alpha]_D^{24} = +38^\circ$ (MeOH, $c = 1.21 \times 10^{-3}$). FT-IR (KBr, ν_{max}): 3323, 2958, 2245, 1683, 1519, 1267, 1172, 1103, 894, 765, 696 cm⁻¹. ¹H NMR (400 MHz, CDCl₃): $\delta = 7.58$ -7.64 (m, 4H), 7.37-7.48 (m,

5H), 7.20 (s, 1H), 4.11 (q, $J = 7.3$ Hz, 1H), 3.40 (dd, $J = 4.8, 8.8$ Hz, 1H), 1.75-1.85 (m, 1H), 1.60-1.66 (m, 1H), 1.39-1.53 (m, 3H), 0.99-1.04 (m, 1H), 0.98 (d, $J = 3.2$ Hz, 3H), 0.97 (d, $J = 3.3$ Hz, 3H), 0.84-0.92 (m, 2H) ppm. ^{13}C NMR (100 MHz, CDCl_3): $\delta = 174.8, 142.5, 140.0, 132.9, 128.9, 128.7, 127.8, 127.7, 127.1, 123.9, 119.6, 63.5$ (q, $J = 28.9$ Hz), 60.0, 42.6, 24.8, 23.0, 21.8, 19.9, 16.8, 16.3 ppm. ^{19}F NMR (376 MHz): $\delta -73.65$ (d, $J = 7.1$ Hz). HRMS (ESI): m/z calcd for $\text{C}_{24}\text{H}_{27}\text{F}_3\text{N}_3\text{O}$ $[\text{M} + \text{H}]^+$: 430.21007; found: 430.21014. HPLC: Lux® 5 μm Cellulose-2, 250 x 4.6 mm, Acetonitrile/Water: 55:45, 0.5 mL min^{-1} , rt: 16.281 min, 206nm; Chiralpak® IC-5 (5 μm), 250 x 4.6 mm, Acetonitrile/Water: 50:50, rt: 20.850 min, 206nm. After HPLC purification *d.e.* > 99%.

5.1.6 *S*-*N*-(1-cyanocyclopropyl)-3-phenyl-2-(((*S*)-2,2,2-trifluoro-1-phenylethyl)amino)propanamide (**16b**)

Silica/ AcOEt: *n*-hexane 30:70 v/v (92% yield). White solid, M.p. 141-143°C. $[\alpha]_{\text{D}}^{24} = +45^\circ$ (MeOH, $c = 1.07 \times 10^{-3}$). FT-IR (KBr, ν_{max}): 3329, 3246, 3032, 2237, 1649, 1539, 1499, 1456, 1263, 1171, 1126, 850, 742, 567 cm^{-1} . ^1H NMR (400 MHz, CDCl_3): $\delta = 7.19$ -7.43 (m, 10H), 3.99 (q, $J = 7.19$ Hz, 1H), 3.43 (m, 1H), 3.11 (dd, $J = 5.43$ and 13.89 Hz, 1H), 3.06 (dd, $J = 6.83$ e 13.89 Hz, 1H), 2.03 (s, 1H), 1.42-1.51 (m, 2H), 1.00-1.04 (m, 1H), 0.86-0.92 (m, 1H) ppm. ^{13}C NMR (100 MHz, CDCl_3): $\delta = 173.4$ 135.8, 133.1, 129.6, 129.3, 129.1, 129.0, 128.6, 127.5, 124.9 (q, $J = 220$ Hz), 119.5, 63.5 (q, $J = 30$ Hz), 60.8, 37.9, 19.9, 16.7, 16.4 ppm. HRMS (ESI): m/z calcd for $\text{C}_{21}\text{H}_{21}\text{F}_3\text{N}_3\text{O}$ $[\text{M} + \text{H}]^+$: 388.16312; found: 388.16379. HPLC: Lux® 5 μm Cellulose-2, 250 x 4.6 mm, Acetonitrile/Water: 50:50, 0.5 mL min^{-1} , rt: 17.500 min, 206nm. After HPLC purification *d.e.* > 99%.

5.1.7 (S)-2-(((R)-1-(4-bromophenyl)-2,2,2-trifluoroethyl)amino)-N-(1-cyanocyclopropyl)-3-phenylpropanamide (**17a**)

Silica/ AcOEt: *n*-hexane 30:70 v/v (78% yield). White solid. $[\alpha]_D^{24} = -51.11^\circ$ (MeOH, $c = 1.35 \times 10^{-3}$). FT-IR (KBr, ν_{\max}): 3339, 3028, 2243, 1686, 1491, 1263, 1170, 1124, 1010, 814, 727, 702 cm^{-1} . ^1H NMR (400 MHz, CDCl_3): $\delta = 7.62$ (s, 1H), 7.26-7.36 (m, 5H), 6.97-7.03 (m, 2H), 6.64 (d, $J = 8.4$ Hz, 2H), 3.67-3.73 (m, 1H), 3.15-3.19 (m, 2H), 2.62 (dd, $J = 10.9, 14.6$ Hz, 1H), 2.07 (d, $J = 9.61$ Hz, 1H), 1.55-1.65 (m, 2H), 1.15-1.30 (m, 2H) ppm. ^{13}C NMR (100 MHz, CDCl_3): $\delta = 173.4, 135.8, 132.0, 131.2, 129.3, 129.2, 129.0, 127.5, 125.6, 123.5, 119.6, 63.1$ (q, $J = 29.4$ Hz), 61.6, 39.3, 20.1, 16.9, 16.5 ppm. ^{19}F NMR (376 MHz): $\delta -74.45$ (d, $J = 7.5$ Hz). HRMS (ESI): m/z calcd for $\text{C}_{21}\text{H}_{19}\text{BrF}_3\text{N}_3\text{O}$ $[\text{M} + \text{H}]^+$: 466.07364; found: 466.07471. HPLC: Lux® 5 μm Cellulose-2, 250 x 4.6 mm, Acetonitrile/Water 60:40, rt: 14.337 min, 206nm. Chiralpak® IC-5 (5 μm), 250 x 4.6 mm, Acetonitrile/Water: 45:55, rt: 30.751 min, 206nm. After HPLC purification *d.e.* > 99%.

5.1.8 (S)-2-(((R)-1-(4-bromophenyl)-2,2,2-trifluoroethyl)amino)-N-(1-cyanocyclopropyl)-3-phenylpropanamide (**17b**)

Silica/ AcOEt: *n*-hexane 30:70 v/v (78% yield). White solid. M.p. 130-133 $^\circ\text{C}$. $[\alpha]_D^{24} = +77^\circ$ (MeOH, $c = 1.21 \times 10^{-3}$). FT-IR (KBr, ν_{\max}): 3339, 3028, 2243, 1686, 1491, 1263, 1170, 1124, 1010, 814, 727, 702 cm^{-1} . ^1H NMR (400 MHz, CDCl_3): $\delta = 7.50$ -7.54 (m, 2H), 7.29-7.38 (m, 3H), 7.12-7.19 (m, 5H), 3.97 (m, 1H), 3.39 (q, $J = 6.24$ Hz, 1H), 3.08 (dd, $J = 3.6, 1.9$ Hz, 1H), 3.05 (dd, $J = 4.6, 11.8$ Hz, 1H), 2.19 (s, 1H), 1.45-1.52 (m, 2H), 0.92-1.06 (m, 2H) ppm. ^{13}C NMR (100 MHz, CDCl_3): $\delta = 173.2, 135.7, 132.2, 132.0, 130.2, 129.2, 129.1, 127.5, 124.6$ (q, $J = 230$ Hz), 123.5, 119.4, 62.82 (q, $J = 29.0$ Hz), 60.7, 38.0, 20.0, 16.7, 16.5 ppm. HRMS (ESI): m/z calcd for $\text{C}_{21}\text{H}_{19}\text{BrF}_3\text{N}_3\text{O}$ $[\text{M} + \text{H}]^+$: 466.07364; found: 466.07471. HPLC: Lux® 5

μm Cellulose-2, 250 x 4.6 mm, Acetonitrile/Water: 60:40, rt: 12.501 min, 206nm. After HPLC purification *d.e.* > 99%.

5.1.9 *(S)*-2-(((*R*)-1-(3-chlorophenyl)-2,2,2-trifluoroethyl)amino)-*N*-(1-cyanocyclopropyl)-3-phenylpropanamide (**18a**)

Silica/ AcOEt: *n*-hexane 30:70 v/v (73% yield). Colorless oil. $[\alpha]_{\text{D}}^{24} = +77.00^{\circ}$ (MeOH, $c = 1.13 \times 10^{-3}$). FT-IR (KBr, ν_{max}): 3336, 3057, 3030, 2250, 1683, 1531, 1475, 1354, 1138, 1101, 897, 790, 761, 700, 514 cm^{-1} . ^1H NMR (400 MHz, CDCl_3): $\delta = 7.66$ (s, 1H), 7.25-7.31 (m, 4H), 7.14 (t, $J = 7.9$ Hz, 1H), 7.00 (m, 2H), 6.78 (s, 1H), 6.70 (d, $J = 7.7$ Hz, 1H), 3.72 (s, 1H), 3.20 (m, 2H), 2.63 (dd, $J = 9.9, 13.5$ Hz, 1H), 2.08 (s, 1H), 1.55-1.65 (m, 2H), 1.17-1.32 (m, 2H) ppm. ^{13}C NMR (100 MHz, CDCl_3): $\delta = 173.4, 135.5, 134.8, 134.2, 130.0, 129.6, 129.1, 128.8, 127.8, 127.7, 126.2, 125.9, 123.1, 119.6, 63.6, 63.3, 63.0, 62.7, 61.7, 39.2, 20.1, 16.9, 16.4$ ppm. HRMS (ESI): m/z calcd for $\text{C}_{21}\text{H}_{20}\text{F}_3\text{N}_3\text{ClO}$ $[\text{M} + \text{H}]^+$: 422.12415; found: 422.12399. HPLC: Lux® 5 μm Cellulose-2, 250 x 4.6 mm, Acetonitrile/Water 50:50, 0.5 mL min^{-1} , rt: 25.316 min, 206nm. After HPLC purification *d.e.* > 99%.

5.1.12 *(S)*-*N*-(1-cyanocyclopropyl)-3-phenyl-2-(((*S*)-2,2,2-trifluoro-1-(4-methoxyphenyl)ethyl)amino)propanamide (**19b**)

Silica/ AcOEt: *n*-hexane 30:70 v/v (90% yield). Colorless oil. $[\alpha]_{\text{D}}^{24} = +59.35^{\circ}$ (MeOH, $c = 1.23 \times 10^{-3}$). FT-IR (KBr, ν_{max}): 3273, 3038, 2237, 1672, 1610, 1533, 1512, 1265, 1145, 1039, 873, 794, 561 cm^{-1} . ^1H NMR (400 MHz, CDCl_3): $\delta = 7.36$ -7.42 (m, 3H), 7.27-7.28 (m, 3H), 7.10-7.13 (m, 2H), 6.88-6.91 (m, 2H), 4.02 (q, $J = 7.2$ Hz, 1H), 3.04 (dd, $J = 4.6, 12.4$ Hz, 1H), 3.00 (dd, $J = 4.1, 12.4$ Hz, 1H), 2.19 (s, 1H), 1.40-1.50 (m, 2H) ppm. ^{13}C NMR (100 MHz, CDCl_3): $\delta = 173.6, 158.9, 133.1, 130.3, 129.6, 129.0, 128.6, 127.5, 126.4, 123.6, 119.5, 114.4,$

63.31 (q, $J = 28.8$ Hz), 55.3, 36.9, 19.9, 16.7, 16.4 ppm. HRMS (ESI): m/z calcd for $C_{22}H_{23}F_3N_3O_2$ $[M + H]^+$: 418.17369; found: 418.17435. HPLC: Lux® 5 μ m Cellulose-2, 250 x 4.6 mm, Acetonitrile/Water: 50:50, 0.5 mL min^{-1} , rt: 18.946 min, 206nm. After HPLC purification *e.e.* > 99%.

5.1.13 *(S)-N-(1-cyanocyclopropyl)-3-(1H-indol-3-yl)-2-(((R)-2,2,2-trifluoro-1-phenylethyl)amino)propanamide (20a)*

Silica/ AcOEt: *n*-hexane 30:70 *v/v* (82% yield). Colourless oil. ^1H NMR (400 MHz, CDCl_3): $\delta = 8.20$ (s, 1H), 7.63 (s, 1H), 7.30-7.25 (m, 2H), 7.11 (m, 2H), 6.99-6.90 (m, 3H), 6.85 (d, $J = 2.0$ Hz, 1H), 6.68 (d, $J = 7.2$ Hz, 1H), 3.69 (q, $J = 7.6$ Hz, 1H), 3.30 (dd, $J = 4.4, 9.2$ Hz, 1H), 3.20 (dd, $J = 4.4, 14.4$ Hz, 1H), 2.87 (dd, $J = 9.2, 14.4$ Hz, 1H), 1.78 (br s, 1H), 1.50 (m, 2H); 1.21-1.06 (m, 2H partially overlapped with water signal). ppm. ^{13}C NMR (100 MHz, CDCl_3): $\delta = 174.7, 136.5, 132.5, 129.2, 128.6, 127.9, 127.1, 127.1, 125.0$ (q, $J = 279.1$ Hz), 123.5, 122.5, 119.9, 119.9, 118.4, 111.5, 109.7, 63.9 ($J = 28.9$ Hz), 61.0, 29.3, 17.0, 16.5 ppm. HRMS (ESI): m/z calcd for $C_{23}H_{21}F_3N_4O$ $[M + H]^+$: 427.1746; found: 427.1741. HPLC: Lux® 5 μ m Cellulose-2, 250 x 4.6 mm, Acetonitrile/Water: 50:50, 0.5 mL min^{-1} , rt: 18.570 min, 206nm.

5.1.14 *(S)-N-(((S)-1-cyano-2-phenylethyl)-4-methyl-2-(((R)-2,2,2-trifluoro-1-phenylethyl)amino)pentanamide (21a)*

Silica/ AcOEt: *n*-hexane 30:70 *v/v* (76% yield). White solid. M.p. 152-154°C. $[\alpha]_D^{24} = -115^\circ$ (MeOH, $c = 1.21 \times 10^{-3}$). FT-IR (KBr, ν_{max}): 3331, 3360, 2966, 2934, 2245, 1672, 1516, 1497, 1267, 1107, 887, 698 cm^{-1} . ^1H NMR (400 MHz, CDCl_3): $\delta = 7.52$ (d, $J = 8.8$ Hz, 1H), 7.26-7.41 (m, 10H), 5.12 (dt, $J = 7.0, 8.8$ Hz, 1H), 3.74-3.77 (m, 1H), 3.15 (d, $J = 7.0$ Hz, 2H), 3.02 (dd, $J = 3.9$ e 9.8 Hz, 1H), 1.93 (d, $J = 9.1$ Hz, 1H), 1.32-1.44 (m, 2H), 1.19-1.25 (m, 1H), 0.80 (d, $J = 6.4$ Hz, 3H), 0.49 (d, $J = 6.3$ Hz, 3H) ppm. ^{13}C NMR (100 MHz, CDCl_3): $\delta = 173.4, 133.8, 133.3, 129.5, 129.3, 129.0, 129.0, 128.0, 127.9, 123.4, 117.9, 63.5$ (q, $J = 29.2$ Hz), 58.4,

42.7, 41.1, 38.9, 24.6, 23.1, 20.8 ppm. HRMS (ESI): m/z calcd for $C_{23}H_{27}F_3N_3O$ $[M + H]^+$: 418.21007; found: 418.20877. HPLC: Lux® 5 μ m Cellulose-2, 250 x 4.6 mm, Acetonitrile/Water: 60:40, 0.5 mL min^{-1} , rt: 14.022 min, 206nm. After HPLC purification *d.e.* > 99%.

5.1.15 *(S)-N-(((S)-1-cyano-2-phenylethyl)-4-methyl-2-(((S)-2,2,2-trifluoro-1-phenylethyl)amino)pentanamide (21b)*

Silica/ AcOEt: *n*-hexane 30:70 *v/v* (76% yield). White solid. M.p. 125-129°C. $[\alpha]_D^{24} = -26^\circ$ (MeOH, $c = 1.26 \times 10^{-3}$). FT-IR (KBr, ν_{max}): 3331, 3360, 2966, 2934, 2245, 1672, 1516, 1497, 1267, 1107, 887, 698 cm^{-1} . 1H NMR (400 MHz, $CDCl_3$): $\delta = 7.30$ -7.39 (m, 6H), 7.19-7.22 (m, 4H), 7.11 (d, $J = 8.77$ Hz, 1H), 4.90-5.00 (m, 1H), 4.00 (q, $J = 7.20$ Hz, 1H), 3.32 (dd, $J = 4.73$ and 8.87 Hz, 1H), 3.00 (dd, $J = 4.37$ and 11.50 Hz, 1H), 2.97 (dd, $J = 4.28$ and 11.50 Hz, 1H), 1.99 (s, 1H), 1.70 (ddq, $J = 6.54$, 8.79 and 13.04 Hz, 1H), 1.51 (ddd, $J = 4.76$, 8.85 and 13.75 Hz, 1H), 1.34 (ddd, $J = 5.58$, 8.92 and 14.21 Hz, 1H), 0.91 (dd, $J = 6.57$ and 9.59 Hz, 6H) ppm. ^{13}C NMR (100 MHz, $CDCl_3$): $\delta = 173.4$, 133.7, 133.5, 129.5, 129.3, 129.1, 129.0, 128.3, 128.0, 124.2, 117.7, 63.6 (d, $J = 28.6$ Hz), 59.2, 42.6, 40.8, 38.8, 24.8, 23.0, 21.8 ppm. HRMS (ESI): m/z calcd for $C_{23}H_{27}F_3N_3O$ $[M + H]^+$: 418.21007; found: 418.20877. HPLC: Lux® 5 μ m Cellulose-2, 250 x 4.6 mm, Acetonitrile/Water: 60:40, 0.5 mL min^{-1} , rt: 13.679 min, 206nm. After HPLC purification *d.e.* > 99%.

5.1.16 *(S)-2-(((R)-1-([1,1'-biphenyl]-4-yl)-2,2,2-trifluoroethyl)amino)-N-(((S)-1-cyano-2-phenylethyl)-4-methylpentanamide (22a)*

Silica/ AcOEt: *n*-hexane 30:70 *v/v* (81% yield). White solid. M.p. 173-176°C. $[\alpha]_D^{24} = -113^\circ$ (MeOH, $c = 1.1 \times 10^{-3}$). FT-IR (KBr, ν_{max}): 3313, 2954, 1672, 1531, 1494, 1332, 1265, 1174,

736, 700 cm^{-1} . ^1H NMR (400 MHz, CDCl_3): δ = 7.57-7.64 (m, 4H), 7.43-7.48 (m, 3H), 7.27-7.41 (m, 8H), 5.13 (dt, J = 7.0 e 8.8 Hz, 1H), 3.82 (q, J = 7.6 Hz, 1H), 3.16 (d, J = 7.0 Hz, 2H), 3.07 (dd, J = 4.0, 9.7 Hz, 1H), 1.34-1.50 (m, 2H), 1.20-1.28 (m, 1H), 0.82 (d, J = 6.3 Hz, 3H), 0.53 (d, J = 6.3 Hz, 3H) ppm. ^{13}C NMR (100 MHz, CDCl_3): δ = 20.9, 23.1, 24.6, 38.9, 41.0, 42.7, 58.5, 63.2 (q, J = 63.19 Hz), 117.9, 123.4, 127.1, 127.7, 127.8, 127.9, 128.5, 128.9, 129.0, 129.3, 132.1, 133.8, 140.0, 142.5 ppm. HRMS (ESI): m/z calcd for $\text{C}_{29}\text{H}_{31}\text{F}_3\text{N}_3\text{O}$ $[\text{M} + \text{H}]^+$: 494.23895; found: 494.24137. HPLC: Lux® 5 μm Cellulose-2, 250 x 4.6 mm, Acetonitrile/Water: 60:40, 0.5 mL min^{-1} , rt: 24.200 min, 206nm. After HPLC purification *d.e.* > 99%.

5.1.17 (*S*)-2-(((*S*)-1-([1,1'-biphenyl]-4-yl)-2,2,2-trifluoroethyl)amino)-*N*-((*S*)-1-cyano-2-phenylethyl)-4-methylpentanamide (**22b**)

Silica/ AcOEt: *n*-hexane 10:90 *v/v* (81% yield). White solid. M.p. 164-166°C. $[\alpha]_{\text{D}}^{24} = -21^\circ$ (MeOH, $c = 1.1 \times 10^{-3}$). FT-IR (KBr, ν_{max}): 3313, 2954, 1672, 1531, 1494, 1332, 1265, 1174, 736, 700 cm^{-1} . ^1H NMR (400 MHz, CDCl_3): δ = 7.57-7.60 (m, 4H), 7.44-7.47 (m, 2H), 7.29-7.42 (m, 6H), 7.21-7.23 (m, 2H), 7.12 (d, J = 8.8 Hz, 1H), 5.04 (dt, J = 6.6, 8.9 Hz, 1H), 4.07 (q, J = 7.2 Hz, 1H), 3.37 (dd, J = 4.7, 8.9 Hz, 1H), 3.02 (d, J = 6.64 Hz, 2H), 1.68-1.77 (m, 2H), 1.52-1.57 (m, 1H), 1.35- 1.40 (m, 1H), 0.96 (d, J = 6.5 Hz, 3H), 0.94 (d, J = 6,6 Hz, 3H) ppm. ^{13}C NMR (100 MHz, CDCl_3): δ = 173.3, 142.4, 140.2, 133.7, 132.3, 129.3, 129.0, 128.9, 128.8, 128.7, 128.0, 127.8, 127.7, 127.2, 124.2, 117.7, 63.4 (q, J = 25 Hz), 59.2, 42.6, 40.8, 38.8, 24.9, 23.1, 21.8 ppm. HRMS (ESI): m/z calcd for $\text{C}_{29}\text{H}_{31}\text{F}_3\text{N}_3\text{O}$ $[\text{M} + \text{H}]^+$: 494.23895; found: 494.24137. HPLC: Lux® 5 μm Cellulose-2, 250 x 4.6 mm, Acetonitrile/Water: 60:40, 0.5 mL min^{-1} , rt: 22.068 min, 206nm. Chiralpak® IC-5 (5 μm), 250 x 4.6 mm, Acetonitrile/Water: 60:40, 0.5 mL min^{-1} , rt: 15.833 min, 206nm. After HPLC purification *d.e.* = 95%.

5.1.18 (2S)-2-[[[(1R)-1-[[[1,1'-biphenyl]-4-yl]-2,2,2-trifluoroethyl]amino]-N-[(1S)-1-cyano-2-phenylethyl]-3-phenylpropanamide (24a)

Silica/ AcOEt: *n*-hexane 10:90 to 50:50 v/v. (64% yield). White solid. ¹H NMR (400 MHz, CDCl₃): δ = 7.65 (d, *J* = 8.5 Hz, 1H), 7.55-7.53 (m, 2H), 7.47-7.744 (m, 2H), 7.41-7.35 (m, 6H), 7.29-7.23 (m, 5H), 6.98 (d, *J* = 7.0 Hz, 2H), 6.76 (d, *J* = 8.0 Hz, 2H), 5.14 (q, *J* = 7.5 Hz, 1H), 3.73 (d, *J* = 8.0 Hz, 1H), 3.24-3.06 (m, 4H), 2.40 (dd, *J* = 10.5, 14.0 Hz, 1H) ppm. ¹³C NMR (100 MHz, CDCl₃): δ = 172.1, 142.1, 140.1, 135.8, 133.8, 129.4, 129.1, 129.0, 129.0, 128.9, 128.1, 128.0, 127.7, 127.4, 127.4, 127.1, 117.8, 71.6, 64.3, 63.0, 61.1, 41.2, 39.2, 38.9 ppm. HRMS (ESI): *m/z* calcd for C₂₉H₃₁F₃N₃O [M + H]⁺: 528.22572; found: 528.22461. HPLC: Chiralpak® IC-5 (5 μm), 250 x 4.6 mm, Acetonitrile/Water: 60:40, 0.5 mL min⁻¹, rt: 22.946 min, 206nm.

5.1.19 (2S)-N-[(1S)-1-cyano-2-phenylethyl]-3-(4-methoxyphenyl)-2-[[[(1R)-2,2,2-trifluoro-1-phenylethyl]amino]propanamide (25a)

Silica/ AcOEt: *n*-hexane 30:70 v/v (75% yield). Colorless oil. [α]_D²⁴ = -51 ° (MeOH, *c* = 1.21 x 10⁻³). FT-IR (KBr, *ν*_{max}): 3352, 3311, 3030, 2839, 2937, 2360, 2245, 1682, 1612, 1514, 1456, 1252, 1126, 885, 750, 696, 548 cm⁻¹. ¹H NMR (400 MHz, CDCl₃): δ = 2.07 (d, *J* = 10.4 Hz, 1H), 2.58 (dd, *J* = 10.9, 14.7 Hz, 1H), 3.06-3.10 (m, 2H), 3.14 (dd, *J* = 8.2, 14.2 Hz, 1H), 3.28 (dd, *J* = 6.8, 14.2 Hz, 1H), 3.36-3.41 (m, 1H), 3.81 (s, 3H), 5.30 (ddd, *J* = 6.8, 8.3 and 9.1 Hz, 1H), 6.64 (d, *J* = 7.5 Hz, 2H), 6.77-6.80 (m, 2H), 6.86-6.89 (m, 2H), 7.14-7.19 (m, 2H), 7.27-7.42 (m, 6H), 7.63 (d, *J* = 9.2 Hz, 1H) ppm. ¹³C NMR (100 MHz, CDCl₃): δ = 38.3, 39.0, 40.6, 55.3, 61.1, 62.6, 62.9, 63.2, 63.5, 114.4, 118.1, 123.3, 126.1, 127.6, 127.8, 127.9, 128.7, 129.0, 129.1, 129.2, 130.0, 132.2, 133.9, 159.0, 172.1 ppm. HRMS (ESI): *m/z* calcd for C₂₇H₂₇F₃N₃O₂

[M + H]⁺: 482.20499; found: 482.20566. HPLC: Lux® 5 µm Cellulose-2, 250 x 4.6 mm, Acetonitrile/Water: 60:40, rt: 28,168 min, 206nm. After HPLC purification *d.e.* > 99%.

5.1.20 (S)-N-((R)-1-cyano-2-phenylethyl)-3-phenyl-2-(((S)-2,2,2-trifluoro-1-phenylethyl)amino)propanamide (**26b**)

Silica/ AcOEt: *n*-hexane 30:70 *v/v* (78% yield). White solid. M.p. 92-96 °C. $[\alpha]_{\text{D}}^{24} = +75^\circ$ (MeOH, *c* = 1.40x 10⁻³). FT-IR (KBr, *v*_{max}): 3360, 3302, 2966, 2935, 2245, 1672, 1514, 1497, 1373, 1267, 1167, 1124, 1109, 887, 756, 696 cm⁻¹. ¹H NMR (400 MHz, CDCl₃): δ = 7.29-7.40 (m, 10H), 7.12-7.20 (m, 6H), 4.98 (dt, *J* = 7.0 and 8.1, 1H), 3.95 (m, 1H), 3.38 (dd, *J* = 6.8, 12.6 Hz, 1H), 3.11 (dd, *J* = 5.3, 13.9 Hz, 1H), 3.06 (dd, *J* = 6.7 and 13.9 Hz, 1H), 2.99 (dd, *J* = 6.0, 12.9 Hz, 1H), 2.95 (dd, *J* = 6.0, 12.9 Hz, 1H), 2.11 (dd, *J* = 4.7, 7.2 Hz, 1H) ppm. ¹³C NMR (100 MHz, CDCl₃): δ = 172.2, 135.8, 133.7, 132.7, 129.6, 129.3, 129.2, 129.1, 129.1, 128.9, 128.7, 128.0, 127.5, 126.0, 123.8, 117.8, 63.4, 63.1, 62.9, 62.7, 59.8, 41.3, 38.4, 37.6 ppm. HRMS (ESI): *m/z* calcd for C₂₆H₂₅F₃N₃O [M + H]⁺: 452.19442; found: 452.19458. HPLC: Lux® 5 µm Cellulose-2, 250 x 4.6 mm, Acetonitrile/Water: 60:40, 0.5mL min⁻¹, rt: 18.102 min, 206nm. After HPLC purification *d.e.* > 99%.

5.1.21 (S)-N-((R)-1-cyano-2-phenylethyl)-3-(4-methoxyphenyl)-2-(((R)-2,2,2-trifluoro-1-phenylethyl)amino)propanamide (**27a**)

Silica/ AcOEt: *n*-hexane 30:70 *v/v* (75% yield). Colorless oil. $[\alpha]_{\text{D}}^{24} = -51^\circ$ (MeOH, *c* = 1.21x 10⁻³). FT-IR (KBr, *v*_{max}): 3352, 3311, 3030, 2839, 2937, 2360, 2245, 1682, 1612, 1514, 1456, 1252, 1126, 885, 750, 696, 548 cm⁻¹. ¹H NMR (400 MHz, CDCl₃): δ = 7.63 (d, *J* = 9.2 Hz, 1H), 7.27-7.42 (m, 6H), 7.14-7.19 (m, 2H), 6.86-6.89 (m, 2H), 6.77-6.80 (m, 2H), 6.64 (d, *J* = 7.5 Hz, 2H), 5.30 (ddd, *J* = 6.8, 8.3, 9.1 Hz, 1H), 3.81 (s, 3H), 3.36-3.41 (m, 1H), 3.28 (dd, *J* =

6.8, 14.2 Hz, 1H), 3.14 (dd, $J = 8.2, 14.2$ Hz, 1H), 3.06-3.10 (m, 2H), 2.58 (dd, $J = 10.9, 14.7$ Hz, 1H), 2.07 (d, $J = 10.4$ Hz, 1H) ppm. ^{13}C NMR (100 MHz, CDCl_3): $\delta = 172.1, 159.0, 133.9, 132.2, 130.0, 129.2, 129.1, 129.0, 128.7, 127.9, 127.8, 127.6, 126.1, 123.3, 118.1, 114.4, 63.5, 63.2, 62.9, 62.6, 61.1, 55.3, 40.6, 39.0, 38.3$ ppm. HRMS (ESI): m/z calcd for $\text{C}_{27}\text{H}_{27}\text{F}_3\text{N}_3\text{O}_2$ $[\text{M} + \text{H}]^+$: 482.20499; found: 482.20566. HPLC: Lux® 5 μm Cellulose-2, 250 x 4.6 mm, Acetonitrile/Water: 60:40, 0.5 mL min^{-1} , rt: 28.168 min, 206 nm. After HPLC purification *d.e.* > 99%.

5.1.22 *(S)-N-((R)-1-cyano-2-phenylethyl)-3-(4-methoxyphenyl)-2-(((S)-2,2,2-trifluoro-1-phenylethyl)amino)propanamide (27b)*

Silica/ AcOEt: *n*-hexane 30:70 *v/v* (75% yield). Colorless oil. $[\alpha]_{\text{D}}^{24} = +48^\circ$ (MeOH, $c = 1.21 \times 10^{-3}$). FT-IR (KBr, ν_{max}): 3352, 3311, 3030, 2839, 2937, 2360, 2245, 1682, 1612, 1514, 1456, 1252, 1126, 885, 750, 696, 548 cm^{-1} . ^1H NMR (400 MHz, CDCl_3): $\delta = 7.31-7.41$ (m, 7H), 7.09-7.21 (m, 6H), 6.89-6.92 (m, 2H), 4.98 (dd, $J = 7.0$ and 15.1 Hz, 1H), 4.01 (q, $J = 7.01$ Hz, 1H), 3.81 (s, 3H), 3.35 (t, $J = 5.8$ Hz, 1H), 2.94-3.07 (m, 4H) ppm. ^{13}C NMR (100 MHz, CDCl_3): $\delta = 172.4, 159.0, 133.8, 132.8, 130.4, 129.6, 129.2, 129.1, 128.9, 128.7, 128.0, 127.5, 126.1, 123.8, 117.8, 114.5, 63.2$ (q, $J = 28.7$ Hz), 59.8, 55.3, 41.3, 38.4, 36.5 ppm. HRMS (ESI): m/z calcd for $\text{C}_{27}\text{H}_{27}\text{F}_3\text{N}_3\text{O}_2$ $[\text{M} + \text{H}]^+$: 482.20499; found: 482.20566. HPLC: Lux® 5 μm Cellulose-2, 250 x 4.6 mm, Acetonitrile/Water: 60:40, 0.5 mL min^{-1} , rt: 19.875 min, 206 nm. After HPLC purification *d.e.* > 99%.

5.1.23 *(R)-N-(1-cyanocyclopropyl)-3-(1H-indol-3-yl)-2-(((S)-2,2,2-trifluoro-1-phenylethyl)amino)propanamide (29a)*

Silica/ AcOEt: n-hexane 30:70 v/v (82% yield). Colourless oil. ^1H NMR (400 MHz, CDCl_3): δ = 8.20 (s, 1H), 7.63 (s, 1H), 7.30-7.25 (m, 2H), 7.11 (m, 2H), 6.99-6.90 (m, 3H), 6.85 (d, J = 2.0 Hz, 1H), 6.68 (d, J = 7.2 Hz, 1H), 3.69 (q, J = 7.6 Hz, 1H), 3.30 (dd, J = 4.4, 9.2 Hz, 1H), 3.20 (dd, J = 4.4, 14.4 Hz, 1H), 2.87 (dd, J = 9.2, 14.4 Hz, 1H), 1.78 (br s, 1H), 1.50 (m, 2H); 1.21-1.06 (m, 2H partially overlapped with water signal). ppm. ^{13}C NMR (100 MHz, CDCl_3): δ = 174.7, 136.5, 132.5, 129.2, 128.6, 127.9, 127.1, 127.1, 125.0 (q, J = 279.1 Hz), 123.5, 122.5, 119.9, 119.9, 118.4, 111.5, 109.7, 63.9 (J = 28.9 Hz), 61.0, 29.3, 17.0, 16.5 ppm. HRMS (ESI): m/z calcd for $\text{C}_{23}\text{H}_{21}\text{F}_3\text{N}_4\text{O}$ [$\text{M} + \text{H}$] $^+$: 427,1746; found: 427,1741. HPLC: Lux® 5 μm Cellulose-2, 250 x 4.6 mm, Acetonitrile/Water: 50:50, 0.5mL min^{-1} , rt: 16.672 min, 206nm.

General Procedure for the synthesis of **15a** and **23b**

A stream of nitrogen was passed through a suspension of aryl bromide (0.18 mmol), the appropriate boronic acid pinacol ester (0.25 mmol), 2M Na_2CO_3 (0.26mL) and DMF (2mL) for 10 min. PdCl_2dppf (8% mol) was then added and the reaction was warmed to 80°C and stirred under nitrogen for 3h. When the reaction was complete, the mixture was cooled to room temperature and extracted with ethyl acetate (3 x 15 mL). The combined ethyl acetate extracts were dried with sodium sulfate and dried under vacuum to give a residue that was purified by chromatography column using a gradient of ethyl acetate/*n*-hexane (10:90 to 50:50) to afford the desired compounds.

5.1.24 (S)-N-(1-cyanocyclopropyl)-4-methyl-2-(((R)-2,2,2-trifluoro-1-(4'-fluoro-[1,1'-biphenyl]-4-yl)ethyl)amino)pentanamide (**15a**)

81% Yield. White solid, M.p. 145-147°C. $[\alpha]_{\text{D}}^{24} = -119^\circ$ (MeOH, $c = 1.11 \times 10^{-3}$). FT-IR (KBr, ν_{max}): 3385, 3312, 2957, 2243, 1686, 1495, 1364, 1254, 1188, 1126, 872, 816, 698 cm^{-1} . ^1H NMR (400 MHz, CDCl_3): δ = 7.64 (s, 1H), 7.53-7.60 (m, 4H), 7.38-7.41 (m, 2H), 7.13-7.17 (m, 2H), 3.88 (q, J = 7.5 Hz, 1H), 3.10 (dd, J = 3.5, 9.6 Hz, 1H), 2.02 (d, J = 7.6 Hz, 1H), 1.48-

1.64 (m, 4H), 1.41-1.47 (m, 1H), 1.20-1.32 (m, 2H), 0.87 (d, J = 6.2 Hz, 3H), 0.61 (d, J = 6.0 Hz, 3H) ppm. ^{13}C NMR (100 MHz, CDCl_3): δ = 174.8, 164.0, 161.5, 141.5, 136.1, 136.1, 132.2, 128.7, 128.6, 128.6, 127.6, 126.3, 123.5, 119.8, 115.9, 115.7, 63.5 (q, J = 29.3 Hz), 59.0, 42.7, 24.7, 23.1, 21.0, 20.1, 16.9, 16.4 ppm. HRMS (ESI): m/z calcd for $\text{C}_{24}\text{H}_{26}\text{F}_4\text{N}_3\text{O}$ [$\text{M} + \text{H}$] $^+$: 448.20065; found: 448.20114. HPLC: Lux® 5 μm Cellulose-2, 250 x 4.6 mm, Acetonitrile/Water: 50:50, 0.5 mL min^{-1} , rt: 28.105 min, 206nm. After HPLC purification *d.e.* > 99%.

5.1.25 *(S)-N-((S)-1-cyano-2-phenylethyl)-4-methyl-2-(((S)-2,2,2-trifluoro-1-(4-(pyrimidin-5-yl)phenyl)ethyl)amino)pentanamide (23b)*

Silica/AcOEt: *n*-hexane 10:90 to 50:50 v/v. (60% yield) followed by HPLC (semi-prep): Column Phenomenex Lux® 5 μm Cellulose-2. Flow 4.72 mL min^{-1} . Eluent B: Acetonitrile; Eluent A: Water. Gradient flow: 0.0-30.0 min 5%-100% of pump B; 30.01-40.00 min 100% of pump B; 40.01-50.0 min 5% of pump B. Peak collected at 21.5 min. White solid. M.p. 59-61 °C. ^1H NMR (400 MHz, CDCl_3): δ = 9.22 (s, 1H), 8.93 (s, 2H), 7.53 (d, J = 8.0 Hz, 2H), 7.37-7.31 (m, 5H), 7.22 (d, J = 7.6 Hz, 2H), 7.07 (d, J = 9.2 Hz, 1H), 5.04 (m, 1H), 4.06 (q, 7.2 Hz, 1H), 3.33 (m, 1H), 3.01 (m, 2H), 1.72 (m, 1H), 1.53 (m, 1H), 1.38 (m, 1H), 0.94 (m, 6H) ppm. ^{13}C NMR (100 MHz, CDCl_3): δ 173.1, 157.8, 155.0, 135.5, 133.7, 129.5, 129.4, 129.1, 128.1, 127.8, 117.7, 63.66 (d, J = 28.7 Hz), 59.7, 42.9, 40.7, 38.8, 24.9, 23.1, 21.8. ^{19}F NMR (376.28 Hz): δ -73.49 (d, J = 6.6 Hz) ppm. Chiralpak® IC-5 (5 μm), 250 x 4.6 mm, Acetonitrile/Water: 50:50, 0.5 mL min^{-1} , rt: 38.264 min, 206nm. After HPLC purification *d.e.* > 99%.

5.1.26 *Synthesis of (S)-N-(1-((1-cyanocyclopropyl)amino)-4-methyl-1-oxopentan-2-yl)benzamide (30)*

First Step: synthesis of (S)-tert-butyl (1-((1-cyanocyclopropyl)amino)-4-methyl-1-oxopentane-2-yl)carbamate (38). Boc-*L*-Leucine (346 mg, 1.5 mmol), HATU (630 mg, 1.65 mmol), 2-aminoacetonitrile hydrochloride (112 mg, 1.2 mmol) were placed in a 25 mL flask. The atmosphere was changed with argon, then DMF (10 mL) was added. The solution was cooled at 0°C, then DIPEA (1066 μ L, 6 mmol) was added dropwise. The reaction was stirred at r.t. for 16 hrs. Ethyl acetate (100 mL) was added and the organic phase was washed with saturated aqueous NaHCO₃ (3x), 0.1 M HCl (3x) and brine (3x), then dried over Na₂SO₄ and evaporated under vacuum. The residue was purified by flash column chromatography on silica using AcOEt: *n*-hexane 40:60 v/v, giving the Boc-*L*-Leucine derivative **38** (80% yield).

Second step: 240 mg (0.82 mmol) of **38** and 6 mL of HCOOH were stirred at r.t. for 16 hrs. The excess of HCOOH was evaporated and the residue was solubilized with H₂O (5 mL). The pH was then adjusted with 1M NaOH at 0°C until 7-8. The water phase was extracted with AcOEt (3x10 mL) and the reunited organic phases were washed with brine (1x). The organic phase was dried over MgSO₄ and evaporated. The residue (~170 mg of a brown oil) was used without purification. Benzoic acid (38 mg, 0.31 mmol), HATU (188 mg, 0.50 mmol), the deprotected amine (~170 mg) were placed in a 10 mL flask. The atmosphere was changed with argon, then DMF (5 mL) was added. The solution was cooled at 0°C, then DIPEA (80 μ L, 0.46 mmol) was added dropwise. The reaction was stirred at r.t. for 16 hrs. Ethyl acetate (50 mL) was added and the organic phase was washed with saturated aqueous NaHCO₃ (3x), 0.1 M HCl (3x) and brine (3x), then dried over Na₂SO₄ and evaporated under vacuum. The purification by flash column chromatography on silica using AcOEt: *n*-hexane 40:60 v/v, gave **30**.

White solid, M.p. 189-191 °C. FT-IR (KBr, ν_{\max}): 3265, 3045, 2959, 2931, 2872, 2243, 1683, 1540, 1541, 1490, 1301, 1327 cm⁻¹. ¹H NMR (500 MHz, DMSO-*d*₆): δ = 8.95 (s, 1H), 8.59 (d, *J* = 10 Hz, 1H), 7.91-7.88 (m, 2H), 7.56-7.51 (m, 1H), 7.60 (m, 1H), 7.48-7.44 (m, 2H), 4.45-4.50 (m, 1H), 1.74-1.60 (m, 2H), 1.52-1.49 (m, 1H), 1.48-1.45 (m, 1H), 1.12-1.09 (m, 2H), 0.97

(d, $J = 8$ Hz, 3H), 0.86 (d, $J = 8$ Hz, 3H) ppm. ^{13}C NMR (100 MHz, $\text{DMSO-}d_6$): $\delta = 174.17, 166.81, 134.35, 131.77, 128.59, 128.03, 121.27, 78.36, 51.87, 40.59, 40.38, 40.17, 39.97, 39.76, 39.55, 39.34, 27.19, 26.93, 24.86, 23.44, 21.76, 20.27, 16.19, 16.03$ ppm. MS (ESI): m/z calcd for $[\text{M} + \text{H}]^+$: 300.170653; found: 300.67 $[\text{M} + \text{H}]^+$. HPLC: Chiralpak® IC-5 (5 μm), 250 x 4.6 mm, Acetonitrile/Water: 45:55, 0.5 mL min^{-1} , rt: 9.895 min, 254 nm.

5.1.27 *N-((S)-1-(((S)-1-cyano-2-phenylethyl)amino)-4-methyl-1-oxopentan-2-yl)benzamide*
(36)

White solid, M.p. 203-205 °C. FT-IR (KBr, ν_{max}): 3286, 3059, 2958, 2931, 2872, 2850, 2245, 1667, 1652, 1529, 1490, 1327, 1246, 1089 cm^{-1} . ^1H NMR (500 MHz, $\text{DMSO-}d_6$): $\delta = 8.84$ (d, $J = 9.5$ Hz 1H), 8.48 (d, $J = 10$ Hz, 1H), 7.92-7.90 (m, 2H), 7.57-7.53 (m, 1H), 7.50-7.46 (m, 2H), 7.33-7.22 (m, 5H), 4.54-4.48 (m, 1H), 3.10 (d, $J = 10$ Hz, 2H), 1.72-1.59 (m, 2H), 1.48-1.41 (m, 1H), 0.9 (m, 2H), 0.90 (d, $J = 8$ Hz, 3H), 0.86 (d, $J = 8$ Hz, 3H) ppm. ^{13}C NMR (100 MHz, $\text{DMSO-}d_6$): $\delta = 172.76, 166.75, 135.92, 134.33, 131.76, 129.82, 128.77, 128.56, 128.01, 127.50, 119.41, 51.95, 42.14, 40.56, 40.36, 40.15, 39.94, 39.73, 39.52, 39.52, 39.31, 37.57, 24.79, 23.38, 21.74$ ppm. MS (ESI): m/z calcd for $\text{C}_{22}\text{H}_{25}\text{N}_3\text{O}_2$ $[\text{M} + \text{H}]^+$: 364.201953; found: 386.18 $[\text{M} + \text{Na}]^+$. HPLC: Chiralpak® IC-5 (5 μm), 250 x 4.6 mm, Acetonitrile/Water: 45:55, 0.5 mL min^{-1} , rt: 17.827 min, 220 nm.

5.2 Enzyme inhibition assays

Enzyme inhibition assays for cruzain and cathepsin L were carried out as reported previously [14,16]. Recombinant cruzain, consisting of the catalytic domain of cruzipain but excluding the carboxy-terminal extension, was expressed and purified as previously described [14]. Enzyme kinetic assays for cruzain were carried out at 37 °C in 200 μL of a solution containing 100 mM acetate buffer pH 5.5, 300 mM NaCl, 5 mM dithiothreitol (DTT), 5% v/v dimethyl sulfoxide (DMSO), 0.01% v/v Triton X-100 and 0.15 nM cruzain. (S)-N-(1-

((cyanomethyl)amino)-1-oxo-3-phenylpropan-2-yl)benzamide was used as a positive control. The rate of the reaction was monitored by the fluorescence emission at 460 nm (excitation at 355 nm) resulting from the hydrolysis of the substrate Z-Phe-Arg-7-amido-4-methylcoumarin. Enzyme kinetic assays for cathepsin L were performed in a similar manner to the cruzain assays at 37 °C in 200 µL of a solution containing 100 mM acetate buffer pH 5.5, 300 mM NaCl, 1 mM dithiothreitol (DTT), 1 mM EDTA, 5% v/v dimethyl sulfoxide (DMSO), 0.01% v/v Triton X-100 and 0.30 nM cathepsin L.

5.3 Assay for anti-trypanosomal activity

Antiparasitic activity against intracellular amastigotes infecting human U2OS cells [20-22]. On day 1 U2OS cells were seeded in black µClear 384-well tissue culture treated polystyrene plates (Greiner Bio-One 781091) at 700 cells in 40 µl of high DMEM media with the aid of a Wellmate Liquid Handler (Thermo-Scientific) and incubated for 24 h at 37 °C/5% CO₂. After 24 hours, trypomastigotes were harvested from the supernatant of LLC-MK2 cell cultures infected with *T. cruzi* Y strain and added in 10 µL of media per well to the U2OS-containing microplate. A total number of 2,800 trypomastigotes were added per well (4 parasites/ 1 host cell). On day 3, compounds were transferred into a polypropylene 384 well intermediate plate (Greiner MasterBlock Deep Well) using a 16-channel manual pipette equipped with disposable tips (ThermoScientific). In order to dilute the compound concentration by 16.6-fold, an intermediate plate was pre-dispensed with 94 µM of DPBS (Hyclone); next, 6 µM of stock compounds were added onto intermediate plate. Finally, 10µL of compound solution were transferred onto U2OS/*T. cruzi*-containing plates, yielding a final concentration of 1% DMSO and a final volume of 60 µl/well. The tested compounds were assayed in dose-response (17 concentration points – 2-fold dilution), with the highest concentration starting at 100 µM, for benznidazole it started at 400µM The experiment was performed in duplicate (i.e. two independent experiments).

At the assay endpoint the plates were fixed with 4% paraformaldehyde (PFA), stained with Draq5 (Biostatus) for 15 min in the dark at room temperature, and five images of each well were acquired at the High Content Imaging System Operetta (PerkinElmer) at 20X magnification. Images were analyzed by the High Content Analysis (HCA) software Harmony (PerkinElmer) for identification, segmentation and quantification of host cell nucleus, cytoplasm and intracellular parasites (figure 1). The HCA provided as output data for all images from one well the total number of cells, total number of infected cells, total number of intracellular parasites and mean number of parasite per infected cell. The ratio of infected to the total number of cells was then calculated, and defined as the Infection Ratio (IR). The raw data for IR values were normalized to 1% DMSO-treated infected (negative control) cells and non-infected cell (positive control) to determine the normalized antiparasitic activity, according to the following formula:

$$\text{Normalized Activity (NA)} = [1 - (\text{Av. IR}_N - \text{Av. IR}_T) / (\text{Av. IR}_N - \text{Av. IR}_P)] \times 100$$

Where:

Av. IR_N: average infection ratio of negative control wells.

Av. IR_P: average infection ratio of positive control wells.

Av. IR_T: average infection ratio of test compound wells (in a given concentration).

The assay quality control was measured by the Z'-factor; calculated for each plate, considering the average and standard deviation of the infection ratio values (IR) from the positive (mock-infected) and negative controls (neat DMSO treated) – according to the following formula (ii):

$$(ii) Z' = 1 - [3 \times (\text{Sdv. IR}_P + \text{Sdv. IR}_N) / (\text{Av. IR}_P - \text{Av. IR}_N)]$$

Where:

Sdv. IR_P: infection ratio standard deviation from the positive control

Sdv.IR_N: infection ratio standard deviation from the negative control

Av.IR_P: average from infection ratio from the positive control

Av.IR_N: average from infection ratio from the negative control

Plates presenting Z' -factor ≥ 0.5 were approved, as it indicates that there is a satisfactory separation between the assay's negative and positive controls.

Concentration-response curves were processed with the GraphPad Prism software, version 6, for generation of sigmoidal dose-response (variable slope) nonlinear curve fitting and determination of EC₅₀ values by interpolation. For this study, EC₅₀ was defined as the compound concentration corresponding to 50% normalized activity. Potency relates to the EC₅₀ – the more potent the compound, the lower is its EC₅₀ – whereas efficacy relates to the maximum observed activity of a compound (in %) – the more efficacious the compound, the closer its maximum activity is from 100%. The CC₅₀ is defined as the compound concentration that reduced the cell ratio to 0.5, when compared to the average number of cells in the negative control wells.

5.4 Measurement of log K_w

Measurement of log K_w, was performed as described previously [45] The High-Performance Liquid Chromatography (Prominence, Shimadzu, Japan) equipment was used with LC 20AT and LC 20AD pumps, DGU-20A5 degasser, SPD-M20A diode arrangement detector (DAD) and auto-injector SIL-20A HT. Chromatographic retention data are expressed as the logarithm of the retention factor, k , defined in equation (5) as where t_r and t_0 are, respectively, the retention times of the analyte of interest and a non-retained compound (acetone).

$$\log k = \log \left(\frac{t_r - t_0}{t_0} \right) \quad (5)$$

To acetone, the void time (t_0) was 1.52 min. The log k values relative to 100% aqueous eluent ($\log k_w$ IAM), experimentally determined on IAM stationary phases, i.e. IAM.PC.DD (100mm \times 4.6mm I. D., 5 μ m, 300 Å - Regis Chemical Company, Morton Grove, IL). It can be used by measuring isocratic retention time using mobile phases containing methanol in percentages (ϕ) ranging from 15 to 50% (v/v). Linear relationships between log k and ϕ values were found for all compounds in the range of eluent composition examined ($r^2 \geq 0.99$) and the intercepts of relation equations [46] were assumed as $\log k_w$ IAM values.

The chromatographic conditions were:

Flow: 1.0 mL/min

Injection volume: 2 μ L

Concentration of analytes: 1 mg.mL⁻¹, It prepared in Methanol:Water 30:70 (v/v)

Wavelength: 206 nm

Temperature 25 °C

6. Ancillary Information

6.1 Competing interest

Authors declare no competing interest

6.2 Acknowledgment

We are indebted to Fundação de Amparo à Pesquisa do Estado de São Paulo – FAPESP (grant #2013/18009-4 and grant #2016/07946-5) for financing this project. One of us (CAM), also wants to acknowledge the National Council for Scientific and Technological Development

(CNPq, grant # 304030/2018-0) in Brazil for scholarships. We thank the two reviewers of the manuscript for their helpful and insightful comments.

7. References

1. Chagas C. Nova tripanozomíaze humana. Estudos sobre a morfologia e o ciclo evolutivo do *Schizotrypanum cruzi* n. gen., n. sp., agente etiológico de nova entidade morbida do homem. *Mem. Inst. Oswaldo Cruz* 1909;1:1-62.
2. Rassi Jr A, Rassi A, Marin-Neto JA. Chagas disease. *Lancet* 2010;391:82-94.
3. Pérez-Molina JA, Molina I. *Lancet* 2018;375:1388-1402.
4. Schmunis GA, Schmunis GA, Yadon ZE. Chagas disease: a Latin American health problem becoming a world health problem. *Acta. Trop.* 2010;115:14-21.
5. Meirelles MNL, Juliano L, Carmona E, Silva SG, Costa EM, Murta ACM, Scharfstein J. Inhibitors of the major cysteine proteinase (GP57/51) impair host cell invasion and arrest the intracellular development of *Trypanosoma cruzi* in vitro. *Mol. Biochem. Parasitol.* 1992;58:175-184.
6. Cazzulo JJ, Stoka V, Turk V. (2001) The major cysteine proteinase of *Trypanosoma cruzi*: a valid target for chemotherapy of Chagas disease. *Curr. Pharm. Design* 2001;7:1143-1156.
7. Engel JC, Doyle PS, Hsieh I, McKerrow JH. Cysteine protease inhibitors cure an experimental *Trypanosoma cruzi* infection. *J. Exp. Med.* 1998;188: 725-734.
8. Ndao M, Beaulieu C, Black WC, Isabel E, Vasquez-Camargo F, Nath-Chowdhury M, Massé F, Mellon C, Methot N, Nicoll-Griffith DA. Reversible cysteine protease inhibitors show promise for a Chagas disease cure. *Antimicrob. Agents Chemother.* 2014;58:1167-1178.

9. Powers JC, Asgian JL, Ekici ÖD, James KE. Irreversible inhibitors of serine, cysteine, and threonine Proteases. *Chem. Rev.* 2002;102:4639-4750.
10. Silva DG, Ribeiro JFR, De Vita D, Cianni L, Franco CH, Freitas-Junior LH, Moraes CB, Rocha JR, Burtoloso ACB, Kenny PW, Leitão A, Montanari CA. A comparative study of warheads for design of cysteine protease inhibitors. *Bioorg. Med. Chem. Lett.* 2017;27:5031-5035.
11. Lowe G, Yuthavong Y. Kinetic specificity in papain-catalysed hydrolyses. *Biochem. J.* 1971;124:107-115.
12. Löser R, Schilling K, Dimmig E, Gütschow M. Interaction of papain-like cysteine proteases with dipeptide-derived nitriles. *J Med Chem.* 2005;48:7688-7707.
13. Beaulieu C, Isabel E, Fortier A, Massé F, Mellon C, Méthot N, Ndao M, Nicoll-Griffith D, Lee D, Park H, Black WC (2010) Identification of potent and reversible cruzipain inhibitors for the treatment of Chagas disease. *Bioorg. Med. Chem. Lett.* 2010;20:7444-7449.
14. Avelar LAA, Camilo CD, de Albuquerque S, Fernandes WB, Gonzalez C, Kenny PW, Leitão A, McKerrow JH, Montanari CA, Orozco EVM, Ribeiro JFR, Rocha JR, Rosini F, Saidel ME. Molecular design, synthesis and trypanocidal activity of dipeptidyl nitriles as cruzain inhibitors. *PLoS. Negl. Trop. Dis.* 2015;9:e3916.
15. Cianni L, Sartori G, Rosini F, De Vita D, Pires G, Lopes BR, Leitão A, Antonio C.B. Burtoloso ACB, Montanari CA. Leveraging the cruzain S3 subsite to increase affinity for reversible covalent inhibitors. *Bioorg. Chem.* 2018;79:285-292.
16. Burtoloso ACB, de Albuquerque S, Furber M, Gomes JC, Gonzalez C, Kenny PW, Leitão A, Montanari CA, Júnior JCQ, Ribeiro JFR, Rocha JR. Anti-trypanosomal activity of non-peptidic nitrile-based cysteine protease inhibitors. *PLoS. Negl. Trop. Dis.* 2017;11:e0005343.

17. Gauthier JY, Chauret N, Cromlish W, Desmarais S, Duong LT, Falguyret J-P, Kimmel DB, Lamontagne S, Leger S, LeRiche T, Lia CS, Masea F, McKay DJ, Nicoll-Griffith DA, Oballa RM, Palmerc JT, Percival MD, Riendeau D, Robichaud J, Rodan GA, Rodan SB, Seto C, Therien M, Truong VL, Venuti MC, Wesolowski G, Young RN, Zamboni R, Black WC. The discovery of odanacatib (MK-0822), a selective inhibitor of cathepsin K. *Bioorg Med Chem Lett.* 2008;18:923-928.
18. Hughes G, Devine PN, Naber JR, O'Shea PD, Foster BS, McKay DJ, Volante RP. Diastereoselective reductive amination of aryl trifluoromethyl ketones and α -amino esters. *Angew. Chem. Int. Ed. Engl.* 2007;46:1839-1842.
19. Chen C, Devine P, Foster B, Hughes G, O'Shea, P. US Patent US20060030731
20. Moraes CB, Giardini MA, Kim H, Franco CH, Araujo-Junior AM, Schenkman S, Chatelain E, Freitas-Junior LH. Nitroheterocyclic compounds are more efficacious than CYP51 inhibitors against *Trypanosoma cruzi*: implications for Chagas disease drug discovery and development. *Sci. Rep.* 2014;4:4703.
21. Bosc D, Mouray E, Cojean S, Franco CH, Loiseau PM, Freitas-Junior LH, Moraes CB, Grellier P, Dubois J. Highly improved antiparasitic activity after introduction of an N-benzylimidazole moiety on protein farnesyltransferase inhibitors. *Eur. J. Med. Chem.* 2016;109:173-186
22. Silva FT, Franco CH, Favaro DC, Freitas-Junior LH, Moraes CB, Ferreira EI. Design, synthesis and antitrypanosomal activity of some nitrofurazone 1,2,4-triazolic bioisosteric analogues. *Eur. J. Med. Chem.* 2016;121:553-560.
23. Hann MM, Leach AR, Harper G. Molecular complexity and its impact on the probability of finding leads for drug discovery. *J. Chem. Inf. Comp. Sci.* 2001;41:856-864.

24. Teague SJ, Davis AM, Leeson PD, Oprea T. The design of leadlike combinatorial libraries. *Angew. Chem. Int. Ed. Engl.* 1999;38:3743-3748.
25. Kenny PW. The nature of ligand efficiency. *J. Cheminf.* 2019;11:8
26. Saxty G, Woodhead SJ, Berdini V, Davies TG, Verdonk ML, Wyatt PG, Boyle RG, Barford D, Downham R, Garrett MD, Carr RA. Identification of inhibitors of protein kinase B using fragment-based lead discovery. *J. Med. Chem.* 2007;50:2293-2296.
27. Maggiora GM. On outliers and activity cliffs – Why QSAR often disappoints. *J. Chem. Inf. Model.* 2006;46:1535-1535.
28. Stumpfe D, Bajorath J. Exploring activity cliffs in medicinal chemistry. *J. Med. Chem.* 2012;55:2932-2942.
29. Hopkins AL, Keserü GM, Leeson PD, Rees DC, Reynolds CH. The role of ligand efficiency metrics in drug discovery. *Nat. Rev. Drug Discov.* 2014;13:105-121.
30. Leach AG, Pilling EA, Rabow AA, Tomasi S, Asaad N, Buurma NJ, Ballard A, Narduolo S. Enantiomeric pairs reveal that key medicinal chemistry parameters vary more than simple physical property based models can explain. *Med. Chem. Comm.* 2012;3:528-540.
31. Schneider N, Lewis RA, Fechner N, Ertl P. Chiral cliffs: investigating the influence of chirality on binding affinity. *ChemMedChem* 2018;13:1315-1324.
32. Bridges AJ, Zhou H, Cody DR, Rewcastle GW, McMichael A, Showalter HD, Fry DW, Kraker AJ, Denny WA. Tyrosine kinase inhibitors. 8. An unusually steep structure-activity relationship for analogues of 4-(3-bromoanilino)-6,7- dimethoxyquinazoline (PD 153035), a potent inhibitor of the epidermal growth factor receptor. *J. Med. Chem.* 1996;39:267-276.

33. Baum B, Muley L, Smolinski M, Heine A, Hangauer D, Klebe G. Non-additivity of functional group contributions in protein-ligand binding: a comprehensive study by crystallography and isothermal titration calorimetry. *J. Mol. Biol.* 2010;397:1042-1054.
34. Biela A, Betz M, Heine A, Klebe G. Water makes the difference: rearrangement of water solvation layer triggers non-additivity of functional group contributions in protein-ligand binding. *ChemMedChem* 2012;7:1423-1434.
35. Kramer C, Fuchs JE, Liedl KR. Strong nonadditivity as a key structure–activity relationship feature: distinguishing structural changes from assay artifacts. *J. Chem. Inf. Model.* 2015;55:483-494.
36. Free SM, Wilson JW. A mathematical contribution to structure-activity studies. *J. Med. Chem.* 1964;53:395-399.
37. Calabrò G, Woods CJ, Powlesland F, Mey ASJS, Mulholland AJ, Michel J. Elucidation of nonadditive effects in protein-ligand binding energies: thrombin as a case study. *J. Phys. Chem. B* 2016;120:5340-5350.
38. Leach AR, Hann MM, Burrows JN, Griffen EJ. Fragment screening: an introduction. *Mol. BioSyst.* 2006;2:429-446.
39. Albert JS, Blomberg N, Breeze AL, Brown AJ, Burrows JN, Edwards PD, Folmer RH, Geschwindner S, Griffen EJ, Kenny PW, Nowak T, Olsson LL, Sanganee H, Shapiro AB. An integrated approach to fragment-based lead generation: philosophy, strategy and case studies from AstraZeneca's drug discovery programmes. *Curr. Top. Med. Chem.* 2007;7:1600-1629.
40. Kenny PW, Leitão A, Montanari CA. Ligand efficiency metrics considered harmful. *J. Comput. Aided Mol. Des.* 2014;28, 699-710.

41. Borges NM, Kenny PW, Montanari CA, Prokopozyk IM, Ribeiro JF, Rocha JR, Sartori GR. The influence of hydrogen bonding on partition coefficients. *J. Comput.-Aided Mol. Des.* 2017;31:163-181.
42. Hammett LP. Linear free energy relationships in rate and equilibrium phenomena. *J. Chem. Soc. Faraday Trans.* 1938;34:156-165.
43. Andrews PR, Craik DJ, Martin JL. Functional group contributions to drug-receptor interactions. *J. Med. Chem.* 1984;27:1648-1657.
44. Scott JS, Waring MJ. Practical application of ligand efficiency metrics in lead optimization. *Bioorg. Med. Chem. Lett.* 2018;26:3006-3015.
45. Quilles Jr JC, Bernardi MDL, Batista PHJ, Silva SCM, Rocha CMR, Montanari CA, Leitão A. Biological activity and physicochemical properties of dipeptidyl nitrile derivatives against pancreatic ductal adenocarcinoma cells. *Anti-Cancer Agents Med. Chem.* 2019;19:112-120
46. Snyder LR, Dolan JW, Gant JR. Gradient elution in high-performance liquid chromatography. *J. Chromatogr.*, 1979;163:3-30.

Sao Carlos, 22 August 2019

Authors declare no conflict of interest.



Carlos Montanari

Journal Pre-proofs

